Julia sets and chaotic tunneling: II

2009 J. Phys. A: Math. Theor. 42 265102

(http://iopscience.iop.org/1751-8121/42/26/265102)

J. Phys. A: Math. Theor. **42** (2009) 265102 (34pp) doi:10.1088/1751-8113/42/26/265102

Julia sets and chaotic tunneling: II

Akira Shudo[1], **Yutaka Ishii**[2] **and Kensuke S Ikeda**[3]

[1] Department of Physics, Tokyo Metropolitan University, Minami-Osawa, Hachioji, Tokyo 192-0397, Japan
[2] Department of Mathematics, Kyushu University, Ropponmatsu, Fukuoka 810-8560, Japan
[3] Department of Physics, Ritsumeikan University, Noji-higashi 1-1-1, Kusatsu 525-8577, Japan

Received 23 June 2008, in final form 14 January 2009
Published 9 June 2009
Online at stacks.iop.org/JPhysA/42/265102

Abstract

Chaotic tunneling is studied based on the complex semiclassical theory as a continuation of the previous paper (Shudo *et al* 2009 *J. Phys. A: Math. Theor.* **42** 265101). In this paper, the nature of complex classical trajectories controlling chaotic tunneling is investigated. Combining the results of numerical investigations and rigorous mathematical considerations based on the theory of complex dynamical systems leads us to a fundamental mathematical theorem which relates the set of complex classical trajectories contributing to the tunneling probability, called the *Laputa chains*, and the chaotic component in the complexified phase space called the *Julia set*. In particular, we demonstrate that the mechanism for tunneling in non-integrable systems is controlled by a dense set of trajectories. This mechanism is radically different from the integrable system where a sparse set of instantons on invariant tori controls tunneling. The physical significance of claims in the fundamental mathematical theorem is numerically examined in detail. On the basis of the numerical studies and the ergodic nature of the Julia set, we finally propose a hypothesis which guarantees the existence of complexified trajectories contributing to the tunneling process in non-integrable systems. The hypothesis supports the following picture of chaotic tunneling: tunneling trajectories pass the dynamical barriers in the real space with the guidance of the stable and unstable sets of the Julia set in the complex space.

PACS numbers: 05.45.Mt, 03.65.Sq, 05.45.−a

(Some figures in this article are in colour only in the electronic version)

1. Introduction and main results

The theoretical understanding of tunneling in systems of more than one dimension is incomplete. An obstacle which makes the multi-dimensional tunneling problem difficult is the presence of chaos in the underlying dynamics. In a preceding paper [1], which we

will refer to as part I, on the basis of semiclassical theory in the time domain, we presented a detailed description of tunneling processes in the presence of chaos by using several kinds of quantum maps and their classical counterparts. By definition, the tunneling phenomenon is a purely quantum transition connecting two regions between which no classical paths exist. To treat tunneling processes in the framework of semiclassical theory, we continue the classical trajectories analytically into the complex domain and treat classical dynamics in the complexified phase space. The initial value representation for complexified trajectories has been employed to show the nature of tunneling trajectories which are caused by underlying chaotic dynamics [1–5].

We define *chaotic tunneling* as the tunneling phenomenon whose complexified semiclassical dynamics is dominated by chaotic dynamics. The number of trajectories contributing to the semiclassical propagator increases as time elapses, in general, at a rate which is more rapid than exponential. An important conclusion of the extensive numerical analyses developed in part I is that the semiclassical propagator is dominated by a restricted class of tunneling trajectories. The subset of dominantly contributing trajectories forms a characteristic chained structure on the initial value plane and the chained object is called a *Laputa chain*[4]. All the characteristics of chaotic tunneling are explained by the Laputa chain [1–3].

Part I was devoted to elucidating features of Laputa chains by extensive numerical investigations for several map systems, and some remarkable features common to all the map systems are extracted. The aim of the present paper is to present mathematical characterization of the set of dominant tunneling trajectories and to numerically examine the physical significance of our mathematical claims. The outlines of mathematical content and corresponding physical examination, which will be elaborated in the present paper, have been presented in our preliminary reports [4] and [5], respectively.

First, we review some key concepts in the semiclassical treatment together with the main results obtained in part I and describe the organization of the present paper. The system with which we discuss chaotic tunneling is the so-called kicked rotor system:

$$H(q,\,p) \equiv H_0(p) + V(q) \sum_{n=-\infty}^{+\infty} \delta(t-n), \tag{1}$$

where δ is the Dirac delta function. The classical equations (Newton's equation of motion) of the system then become

$$\begin{cases} \dfrac{\mathrm{d}p}{\mathrm{d}t} = -V'(q) \displaystyle\sum_{n=-\infty}^{+\infty} \delta(t-n), \\ \dfrac{\mathrm{d}q}{\mathrm{d}t} = H_0'(p). \end{cases} \tag{2}$$

The system of equations above gives a discontinuous flow in complex two-dimensional $(q,\,p)$-space $\mathbb{C}^2$, and one obtains the corresponding time-one map $(q(n-0),\,p(n-0)) \mapsto (q(n+1-0),\,p(n+1-0))$ of this flow, which then becomes the area-preserving map

$$g : (p, q) \longmapsto (H_0'(p) - V'(q), q + H_0'(p - V'(q))). \tag{3}$$

In part I, we examined several maps by taking H_0 and V in different forms. In the present paper, we will employ the cubic potential:

$$H_0(p) = p^2/2 \qquad \text{and} \qquad V(q) = aq - q^3/3 \tag{4}$$

[4] The name Laputa is taken from the floating island in the famous story *Gullivers' Travels*. Laputa chains float in the imaginary space.

as a standard model, because the cubic potential is simple and it describes the typical situation of chaotic tunneling through a potential barrier. In particular, by the affine change of coordinate $(q, p) = (y - 1, y - x)$, the time-one map of the cubic potential is transformed to the Hénon map:

$$f : (x, y) \longmapsto (y, y^2 + (1 - a) - x), \tag{5}$$

which has been extensively studied by many authors from mathematical perspective. The investigation from the complex dynamical point of view has been developed in the last decade (see, for example [6–9] and the references therein) by using pluripotential theory, the theory of currents, etc. In this paper, we will apply the fruits of these mathematical results to the physics problem which was numerically investigated in part I, i.e., the characterization of tunneling trajectories represented by the Laputa chain. Given the initial and final quantum states, which are specified by real numbers α and β, respectively, the semi-classical propagator of the map is expressed as

$$K_n^{\mathrm{sc}}(\alpha; \beta) \equiv \sum_{(q,p)\in\mathcal{M}_n^{\alpha,\beta}} A_n(q, p) \exp\left\{\frac{\mathrm{i}}{\hbar} S_n(q, p)\right\}, \tag{6}$$

where S_n denotes the *classical action*

$$S_n(q, p) \equiv \sum_{j=1}^{n} \{H_0(p_j) + V(q_{j-1}) + q_{j-1}(p_j - p_{j-1})\} \tag{7}$$

along the classical trajectory $(q_j, p_j) \equiv g^j(q, p)$. The amplitude factor $A_n(q, p)$ is associated with stability of each orbit and roughly given as $\|Dg^n(q, p)\|^{-\frac{1}{2}}$. The summation is taken for all $(q, p) \in \mathcal{M}_n^{\alpha,\beta}$ where

$$\mathcal{M}_n^{\alpha,\beta} \equiv \{(q, p) \in \mathbb{C}^2 : p = \alpha \text{ and } p_n = \beta\} \tag{8}$$

for given $\alpha, \beta \in \mathbb{R}$. Here, α is a fixed initial condition for the momentum p and β is a fixed final condition. We can neither fix q nor q_n because of the uncertainty principle. It can be easily seen that the cardinality of the set $\mathcal{M}_n^{\alpha,\beta}$ does not exceed 2^n because g is a polynomial of degree 2.

In the above representation, the classical action (7) is a function of initial values q and p. It is, however, often convenient to regard the action S_n as a function of two boundary values $\alpha = p$ and $\beta = p_n$ instead of the initial values. Hereafter, we use the notation $S_n(\alpha, \beta)$, when we regard the classical action as a function of the two boundary values, and distinguish it from $S_n(q, p)$, which is used when the action is taken as a function of initial values. Then $S_n(\alpha, \beta)$ has the property of a generating function for the canonical conjugate pairs

$$q = \frac{\partial S_n(\alpha, \beta)}{\partial \alpha}, \qquad q_n = -\frac{\partial S_n(\alpha, \beta)}{\partial \beta}. \tag{9}$$

We may define $\mathcal{M}_n^{\alpha,\beta}$ more generally as follows: let $A(q, p)$ and $B(q, p)$ be two polynomials in variables (q, p), which are the classical counterparts of physical quantities controlling the initial and final quantum states, respectively. Since the initial and final states are fixed to real values α and β, we can put

$$\mathcal{M}_n^{\alpha,\beta} \equiv \{(q, p) \in \mathbb{C}^2 : A(q, p) = \alpha \text{ and } B(q_n, p_n) = \beta\}. \tag{10}$$

The original definition of $\mathcal{M}_n^{\alpha,\beta}$ in equation (6) can be recovered as the case $A(q, p) = B(q, p) = p$. Another important example would be $A(q, p) = a_{pp}p^2/2 + a_{pq}pq + a_{qq}q^2/2$, where a_{pp}, a_{pq}, a_{qq} are certain constants and $B(q, p) = q$. (See section 2 and appendix A of part I for more details. We say that the trajectory starting from (q, p) *asymptotically contributes*

to the tunneling transition if the modulus of $\lim_{n\to\infty} \exp\{\frac{\mathrm{i}}{\hbar} S_n(q, p)\}$ has a bounded positive value, i.e., if the imaginary part of $S_n(q, p)$ converges as $n \to \infty$.

As stated above, the *Laputa chain* is a set of dominantly contributing trajectories and it forms a characteristic chained structure on the initial value plane. Laputa chains show some remarkable features. We quote here the three main numerical observations summarized in section 4 of part I (omitting some non-essential statements).

Numerical observation (i)

The dominantly contributing part of Laputa chain, which is called the trunk chain, is quasi-real. Quasi-real means that the trajectory from the trunk part lands very close to the real plane. The trunk chain contributes to the wavefunction with almost the same magnitude, which is observed as the plateau of the tunneling wavefunction characteristic in the chaotic range.

Numerical observation (ii)

Every branch in the Laputa chain splits into each time step. Such splittings result in the bifurcation of Laputa chain into a branched structure with higher order chains as the branches. The branches also further bifurcate into higher order branches, and in the limit of $n \to \infty$, *the trunk part of the branched Laputa chain, which forms a branched trunk chain, morphologically converges to form a self-similar structure.*

Numerical observation (iii)

The itinerary of the trajectories launched from the morphologically converging trunk chain also converges in the limit of $n \to \infty$. *In particular, in the final stage they approach exponentially to the real plane, which means that* Im S_n *along the trajectory converges absolutely as* $n \to \infty$.

Summarizing the above observations, we proposed in section 4 of I an empirical definition of Laputa chain: consider the whole set of the initial conditions of the tunneling trajectories. Laputa chains are subsets having the following properties:

(1) *They asymptotically converge in shape in the initial value plane.*
(2) *The imaginary part of action along the trajectories leaving them converge absolutely.*

Further, on the basis of the definition, we made the conjecture that the Laputa chains are closely related to the *forward filled Julia set* K^+, where K^+ consists of the points for which forward iterations of g are bounded. Its boundary $J^+ = \partial K^+$ is called the *forward Julia set* , a key notion in the theory of complex dynamical systems. (Precise definitions of K^+ and J^+ are provided in the following section.) We numerically confirmed the similarity between Laputa chains and the slice of K^+ by the initial manifold $A(q, p) = \alpha$.

However, our conjecture is so far based only on numerical observations and lacks rigorous mathematical basis. We want to ask the following questions:

(a) How can the morphologically converging components in the set of initial conditions and the convergence in the imaginary action be described using mathematical concepts?
(b) How are the Laputa chains connected with K^+ and, in particular, J^+?

In section 2 we will give a partial mathematical answer to the above questions. As an answer to question (a), we prove in subsection 2.2, proposition 2.7, the convergence of $\mathcal{M}_n^{\alpha,\beta}$ in the Hausdorff topology (which roughly means the convergence of the sequence of shapes of $\mathcal{M}_n^{\alpha,\beta}$ in the limit of $n \to \infty$).

Next, in subsection 2.3 we propose a mathematical definition of the Laputa chains, denoted by $\mathcal{C}_{\text{Laputa}}$, as the set of points $\mathcal{M}_n^{\alpha,\beta}$ in the limit of $n \to \infty$ for which the imaginary part of the action converges absolutely, so that it asymptotically contributes to the tunneling transition.

An answer to the question (b) is then given in the following main theorem (for a preliminary report without proof, see [4]).

Main theorem. *Let g be the time-one map (3) on $\mathbb{C}^2$ for the kicked rotor with cubic potential. Then, the following hold.*

(i) If $h_{\mathrm{top}}(g|_{\mathbb{R}^2}) > 0$, then $K^+ \supset \overline{\mathcal{C}_{\mathrm{Laputa}}} \supset J^+$.
(ii) If g is hyperbolic and $h_{\mathrm{top}}(g|_{\mathbb{R}^2}) > 0$, then $\overline{\mathcal{C}_{\mathrm{Laputa}}} = J^+$.
(iii) If g is hyperbolic and $h_{\mathrm{top}}(g|_{\mathbb{R}^2}) = \log 2$, then $\mathcal{C}_{\mathrm{Laputa}} = J^+$.

Here h_{top} is topological entropy and $\overline{X}$ indicates the closure of X. This theorem is treated in section 2.

We note that the condition $h_{\mathrm{top}}(g|_{\mathbb{R}^2}) > 0$ is equivalent to the existence of a horseshoe (hence the existence of chaos) in $\mathbb{R}^2$ by a theorem of Katok in dimension two [10] and the forward Julia set J^+ is a large set in the sense of potential theory. Thus, the main theorem suggests that when the underlying classical dynamics is chaotic a bunch of paths in $\mathbb{C}^2$ contributes to the tunneling phenomena.

This mechanism is unlike that in the integrable case where a sparse set of instanton solutions dominates the tunneling transition probability. The main theorem concerns the asymptotic limit $n \to \infty$, whereas in the numerical studies n is large but finite. In section 3, we re-examine in detail how the claims in the theorem correspond to the set $\mathcal{M}_n^{\alpha,\beta}$ for large but finite n. In subsections 3.1, 3.2 and 3.3 we see how each of the three claims in the main theorem, (iii), (ii) and (i), respectively, manifests in qualitatively different tunneling paths depending on the different conditions on the map g. Firstly, in subsection 3.1 the most ideal case where the map is hyperbolic in the real plane is examined, and it is shown that the claim (iii) exactly holds for the set of tunneling trajectories observed on the entrance side. Secondly, case (ii), where the map is hyperbolic in the complex phase space, is examined in subsection 3.2, and it is shown that the claim implies a new class of tunneling trajectories itinerating over complex saddles. Thirdly, in subsection 3.3 it is shown that even in non-hyperbolic situation, in which chaos and invariant KAM circles are coexistent, the most general claim (i), which is strengthened by supposing a numerically confirmed conjecture, agrees well with the essential features of dominantly contributing tunneling trajectories in the initial plane. We also discuss, for each of the three cases, what happens on the exit side of contributing trajectories based on the implications of mathematical claims in section 3, and an important relationship between the set

$$\mathcal{L}_n^{\alpha,\beta} \equiv \{(q_n, p_n) \in \mathbb{C}^2 : A(q, p) = \alpha \text{ and } B(q_n, p_n) = \beta\}, \tag{11}$$

which supports the semiclassical wavefunction, and the backward Julia set J^- is discussed.

In section 4, we focus on the role of complex chaos in the Julia set. With a hypothesis on the nature of the Julia set, we discuss the significance of complex chaos as the underlying mechanism of chaotic tunneling on the basis of its ergodic properties. It is also shown that the location of dominant tunneling paths in phase space is related to that of the natural boundaries of KAM circles. We are finally led to a general hypothesis governing the organization of tunneling paths in non-integrable systems, which is in sharp contrast to the instanton mechanism in integrable systems: the dominant tunneling trajectories are attracted by the Julia set in the real phase space being guided by J^+ and finally land close to J^-.

Section 5 is devoted to concluding the paper.

2. Mathematical characterizations

2.1. Dynamics of the Hénon map

In this section we review some basic facts concerning the dynamics of the Hénon map which will be used later. To begin with, we take the following normal form of the Hénon map:

$$f \equiv f_{c,b} : (x, y) \longmapsto (y, y^2 + c - bx), \tag{12}$$

which is defined on the complex phase space $\mathbb{C}^2$. It is easy to see that f has a polynomial inverse, so both the forward and backward iterations can be considered. In the tunneling problem the parameters are taken to be $b = 1$ and $c = 1 - a \in \mathbb{R}$, and in this case the Hénon map defines dynamics both in $\mathbb{R}^2$ and in $\mathbb{C}^2$.

For a complex Hénon map f, we define the *forward* (resp. *backward*) *filled Julia set* K^+ (resp. K^-) of f to be the set of points in $\mathbb{C}^2$ whose forward (resp. backward) orbits are bounded, i.e.

$$K^{\pm} \equiv \{(x, y) \in \mathbb{C}^2 : \{f^{\pm n}(x, y)\}_{n \geqslant 0} \text{ is bounded in } \mathbb{C}^2\}.$$

The *forward Julia set* J^+ (resp. the *backward Julia set* J^-) of f is the boundary of K^+ (resp. K^-), i.e.

$$J^{\pm} \equiv \partial K^{\pm}.$$

Finally, we call

$$J \equiv J^+ \cap J^-$$

the *Julia set* of f.

The Hénon map has the following filtration property [6, 22]. Let us introduce

$$\begin{aligned} V^+ &= \{(x, y) \in \mathbb{C}^2 : |y| > R, |y| > |x|\}, \\ V^- &= \{(x, y) \in \mathbb{C}^2 : |x| > R, |x| > |y|\}. \end{aligned} \tag{13}$$

For a sufficiently large $R > 0$ it can be shown that $f(V^+) \subset V^+$ and $f^{-1}(V^-) \subset V^-$. Furthermore, once an orbit drops into V^+ (resp. V^-), it diverges to infinity by the forward (resp. backward) iterations. In other words,

$$\bigcup_{n=0}^{\infty} f^{\mp n}(V^{\pm}) = \mathbb{C}^2 \setminus K^{\pm}. \tag{14}$$

Let $X \in \mathbb{C}^2$ be a saddle periodic point, Then, by using an argument on normal family, we get $W^s(X) \subset J^+$ and $W^u(X) \subset J^-$ for its stable and unstable manifolds.

A powerful tool to investigate the nature of Julia set is the *Green function* for $K^{\pm}$:

$$G^{\pm}(x, y) \equiv \lim_{n \to +\infty} \frac{1}{2^n} \log^+ \| f^{\pm n}(x, y) \| \tag{15}$$

which is shown to be continuous and plurisubharmonic on $\mathbb{C}^2$. Thus, by identifying $(x, y) = (z_1, z_2)$, we can apply the dd^c-operator:

$$dd^c u \equiv 2\mathrm{i} \sum_{j,k=1}^{2} \frac{\partial^2 u}{\partial z_j \partial \overline{z}_k} \, \mathrm{d}z_j \wedge \mathrm{d}\overline{z}_k$$

to $G^{\pm}(x, y)$ in the sense of distribution so as to get the $(1, 1)$-currents:

$$\mu^{\pm} \equiv \frac{1}{2\pi} dd^c G^{\pm}. \tag{16}$$

Here, a function $u : U \to \{-\infty\} \cup \mathbb{R}$ defined on a domain $U \subset \mathbb{C}^2$ is called *plurisubharmonic* if (i) u is upper semi-continuous, and (ii) for any complex line $\mathbb{C} \subset \mathbb{C}^2$ the restriction of u to $U \cap \mathbb{C}$ is subharmonic. The definition of a subharmonic function is also given as follows: a function $u : U \to \{-\infty\} \cup \mathbb{R}$ defined on a domain $U \subset \mathbb{C}$ is called *subharmonic* if (i) u is upper semi-continuous and (ii) for any disc $D \subset U$ we have $u \leqslant h$ on D, where h is a harmonic function so that $u = h$ on the boundary of D. A significance of this property is that $\triangle u$ becomes a measure on U.

The meaning of the Green function can be understood by the analogy of the electrostatic potential of a perfect conductor. The charge on a perfect (earthed) conductor is distributed over the surface. Once the potential function is known, the surface distribution of charge can be computed by applying the Laplacian to the electrostatic potential, and thus we can identify the surface of the conductor as the support of the charge distribution. The Green function just corresponds to the potential function, and the dd^c to the Laplacian operator. μ^+ (resp. μ^-) plays the role of the equilibrium charge distribution localized on the boundary of K^+ (resp. K^-), and thus the support of μ^+ (resp. μ^-) is the boundary of K^+ (resp. K^-), namely J^+ (resp. J^-). Indeed it can be easily shown that

$$\text{supp}\ \mu^{\pm} = J^{\pm}. \tag{17}$$

Note that $G^+(x, y) = 0$ if and only if $(x, y) \in K^+$ (resp. $G^-(x, y) = 0$ if and only if $(x, y) \in K^-$); this corresponds to the null electrostatic potential inside the perfect conductor.

We remark that the wedge product

$$\mu = \mu^+ \wedge \mu^- \tag{18}$$

is well defined and becomes a hyperbolic invariant measure with maximal entropy, whose support $J^* \equiv \text{supp}(\mu) \subset J$ provides an invariant set on which typical chaotic motions with positive Lyapunov exponent, mixing and ergodic properties, take place [8].

As principal tools, we will employ the following results which have been established by Bedford and Smillie [6, 7] and Fornaess and Sibony [11]. It relates the repeated iteration (repeated pull-back) of the current supported by a certain class of complex manifolds and the currents $\mu^{\pm}$.

Theorem 2.1. *Let M be a complex one-dimensional locally closed submanifold in either J^+ or an algebraic set in $\mathbb{C}^2$. Then, there is a constant $c > 0$ so that*

$$\lim_{n\to+\infty} \frac{1}{2^n}[f^{-n}M] = c\mu^+ \tag{19}$$

in the sense of current, where $[M]$ is the current of integration of M.

The theorem above can be applied to a piece M of the stable manifold $W^s(X)$ of any saddle X, because $W^s(X) \subset J^+$. One then obtains

Corollary 2.2 (Bedford–Smillie [7]). *For any saddle X, $W^s(X)$ is dense in J^+, namely $J^+ = \overline{W^s(X)}$.*

The above result implies that the stable manifold of only one single saddle can very well approximate the whole J^+. It further means that in an arbitrary close neighborhood of any point in $W^s(X)$ there exists a part of the stable manifold of any another saddle. Such a feature can never be expected as long as the dynamics is confined into the real phase space in which the stable manifolds of different saddles may be separated by KAM invariant circles; such a feature is realized thanks to the extension of phase space into the complex domain.

One concept which allows us to handle the dynamics easily is the hyperbolicity of a map f. We say that f is *hyperbolic* when J is a hyperbolic set for f, i.e. there are a

continuous f-invariant splitting of the tangent bundle $T\mathbb{C}^2 = E^u \oplus E^s$ over the Julia set J, a metric in $T\mathbb{C}^2$, and constants $C > 0$ and $0 < \lambda < 1$ such that

$$\left\| Df_X^{-n}\big|_{E_X^u} \right\| < C\lambda^n \qquad \text{and} \qquad \left\| Df_X^{n}\big|_{E_X^s} \right\| < C\lambda^n \tag{20}$$

for all $n > 0$ and $X \in J$.

First, the following can be proven:

Theorem 2.3 (Bedford–Smillie [6]). *If f is hyperbolic and $|b| = 1$, then $K^{\pm}$ have no interior and thus $K^+ = J^+$ and $K^- = J^-$.*

A Hénon mapping is said to be *real* if b and c are real numbers. In this case f is a well-defined dynamical system in the real phase space $\mathbb{R}^2$ which will be denoted by $f|_{\mathbb{R}^2}$. The next theorem gives a connection between the dynamics of Hénon mappings on $\mathbb{C}^2$ and that on $\mathbb{R}^2$.

Theorem 2.4 (Bedford–Lyubich–Smillie [9]). *Suppose that f is real. Then, $h_{\text{top}}(f|_{\mathbb{R}^2}) = \log 2$ if and only if $K \subset \mathbb{R}^2$, where $K \equiv K^+ \cap K^-$.*

Remark 2.5. We remark that under the assumptions that f is real, hyperbolic and $|b| = 1$, the condition $K \subset \mathbb{R}^2$ can be replaced by $J \subset \mathbb{R}^2$ because $K = K^+ \cap K^- = J^+ \cap J^- = J$.

As we have seen before, the complex Hénon map g associated with the kicked rotor with the cubic potential is affinely conjugate to some $f_{c,b}$ which should satisfy $b = 1$ and $c \in \mathbb{R}$. Thus, the results which are valid for $f_{c,b}$ with these conditions are also valid for our time-one map g. In what follows the invariant sets and invariant currents ($K^{\pm}$, $J^{\pm}$, J, $\mu^{\pm}$, etc) mean those for g if not specified.

2.2. $\mathcal{M}_n^{*,\beta}$ and J^+

In this subsection and the next, we develop a mathematical definition of Laputa chains based upon numerical characterizations for them presented in section 4 of I. First, in this subsection, we investigate the asymptotic behavior of the sequence of the sets defined by equation (8) or more generally by equation (10), namely

$$\mathcal{M}_n^{\alpha,\beta} \equiv \{(p, q) \in \mathbb{C}^2 : (p_0, q_0) \in \mathcal{A}_\alpha \text{ and } (p_n, q_n) \in \mathcal{B}_\beta\} \tag{21}$$

in $\mathbb{C}^2$, where $(p_n, q_n) = g^n(p, q)$. Here, we have introduced the initial manifold $\mathcal{A}_\alpha$ and the final manifold $\mathcal{B}_\beta$, which represent respectively the initial and final boundary conditions

$$\mathcal{A}_\alpha = \{(q, p) \in \mathbb{C}^2 : A(q, p) = \alpha\}, \qquad \mathcal{B}_\beta = \{(q, p) \in \mathbb{C}^2 : B(q, p) = \beta)\}. \tag{22}$$

Recall that the set of initial points contributing to the semiclassical propagator is $\mathcal{M}_n^{\alpha,\beta}$. The numerical observation (ii) asserts that $\mathcal{M}_n^{\alpha,\beta}$ contains components called Laputa chains, which exhibit strong tendency of converging, non-uniformly in general, to some asymptotic limit. Hence we first consider how we can obtain a converging structure out of the sequence of the set $\mathcal{M}_n^{\alpha,\beta}$, which does not in general have converging property.

Instead of $\mathcal{M}_n^{\alpha,\beta}$ we consider the sequence of hyperplanes

$$\mathcal{M}_n^{*,\beta} \equiv \{(q, p) \in \mathbb{C}^2 : B(q_n, p_n) = \beta\}.$$

The intersection (slice) of $\mathcal{M}_n^{*,\beta}$ by the initial manifold $\mathcal{A}_\alpha$ gives $\mathcal{M}_n^{\alpha,\beta}$. Letting n go to infinity for each $\beta \in \mathbb{R}$, we relate $\mathcal{M}_n^{*,\beta}$ to the forward Julia set J^+ of g.

To consider a 'limit' of a sequence of sets such as $\left\{\mathcal{M}_n^{*,\beta}\right\}_n$ we introduce the Hausdorff distance:

Definition 2.6. *Let (X, d) be a metric space and $\mathcal{C}(X)$ be the set of all non-empty compacts in X. For A and B in $\mathcal{C}(X)$ we set*

$$\delta(A, B) \equiv \inf\{\varepsilon > 0 : [A]_\varepsilon \supset B \text{ and } [B]_\varepsilon \supset A\} \tag{23}$$

and call it the Hausdorff distance between A and B, where $[A]_\varepsilon$ means the ε-neighborhood of A:

$$[A]_\varepsilon \equiv \left\{y \in X : d(x, y) < \varepsilon \text{ for some } x \in A\right\}.$$

We examine the convergence of the sequence $\mathcal{M}_n^{*,\beta}$ in the Hausdorff topology. It is known that the space $(\mathcal{C}(X), \delta)$ is compact when X is compact. On the other hand, the space $\mathbb{C}^2$ is not compact, so we make the one-point compactification $\mathbb{C}^2 \cup \{\infty\} \cong S^4$ and regard it as a compact metric space (with the spherical metric). Thus, for a closed subset $Y \subset \mathbb{C}^2$, $\widehat{Y} \equiv Y \cup \{\infty\}$ becomes compact in S^4. Conversely, for a set $\widehat{Y} \subset S^4$ with $\infty \in \widehat{Y}$, we put $Y \equiv \widehat{Y} \setminus \{\infty\}$. Note that the spherical metric is equivalent to the usual Euclidean metric in a fixed bounded region of $\mathbb{C}^2$.

For the proof of the next proposition, we do not need the hyperbolicity assumption.

Proposition 2.7. *There is a subsequence $\{n_i\} \subset \mathbb{N}$ such that*

$$\lim_{n_i \to \infty} \widehat{\mathcal{M}_{n_i}^{*,\beta}} \supset \widehat{J^+} \tag{24}$$

where the limit is taken in the Hausdorff topology of $\mathcal{C}(S^4)$. In fact, the conclusion holds for every subsequence $\{n_i\} \subset \mathbb{N}$ for which the limit of $\widehat{\mathcal{M}_{n_i}^{*,\beta}}$ exists.

Taking the slice of the sets on both sides of equation (24) with the hyperplane $\mathcal{A}_\alpha$, we have a relationship between the limit of $\mathcal{M}_{n_i}^{\alpha,\beta}$ and the slice $J^+ \cap \mathcal{A}_\alpha$. This is a partial verification of the numerical observation (ii).

For the proof we first show the following lemma.

Lemma 2.8. *For every subsequence $\{n_i\} \subset \mathbb{N}$, we have*

$$\bigcap_{m=0}^{\infty} \overline{\bigcup_{n_i > m} \widehat{\mathcal{M}_{n_i}^{*,\beta}}} \supset \widehat{J^+}. \tag{25}$$

Proof. Recall the definition (2.2) of $\mathcal{M}_n^{*,\beta} \equiv \{(q, p) \in \mathbb{C}^2 : g^n(q, p) \in \mathcal{B}_\beta\}$. We easily obtain that $\mathcal{M}_{n+k}^{*,\beta} = g^{-k}\mathcal{M}_n^{*,\beta}$. Take $m > 0$ arbitrarily. Let ε be a positive real number and let $X \in \operatorname{supp} \mu^+ = J^+$. Then, for the ε-neighborhood U of X there is a $(1, 1)$-test form ψ with $\operatorname{supp} \psi \subset U$ and $\mu^+(\psi) > 0$. By theorem 2.1, we get $\left[\mathcal{M}_{n_k}^{*,\beta}\right](\psi)0$ for a large $n_k > m$, which means $U \cap \mathcal{M}_{n_k}^{*,\beta} \neq \emptyset$. This shows that $X \in \overline{\bigcup_{n_i > m} \mathcal{M}_{n_i}^{*,\beta}}$. Because this is valid for any m, we obtain the desired proof. □

Proof of proposition 2.7. Because the space $(\mathcal{C}(S^4), \delta)$ is compact, there is a subsequence $\{n_i\} \subset \mathbb{N}$ so that $\widehat{\mathcal{M}_{n_i}^{*,\beta}}$ converges. By choosing a new subsequence from $\{n_i\}$ if necessarily, we may assume that

$$\delta\left(\widehat{\mathcal{M}_{n_i}^{*,\beta}}, \widehat{\mathcal{M}_{n_j}^{*,\beta}}\right) < \max\{1/i, 1/j\}. \tag{26}$$

Now, getting the conclusion is a standard argument (as in Blaschke's selection theorem) but for completeness we show the proof here. What we should show is that the limit of $\widehat{\mathcal{M}_{n_i}^{*,\beta}}$ coincides with the left-hand side of (25).

By (26), we see $\widehat{\mathcal{M}^{*,\beta}_{n_i}} \subset \left[\widehat{\mathcal{M}^{*,\beta}_{n_j}}\right]_{1/j}$ when $i > j$. So we first obtain $\overline{\bigcup_{i>j}^{\infty} \widehat{\mathcal{M}^{*,\beta}_{n_i}}} \subset \left[\widehat{\mathcal{M}^{*,\beta}_{n_j}}\right]_{1/j}$, which means that

$$\bigcap_{m=0}^{\infty} \overline{\bigcup_{n_i>m} \widehat{\mathcal{M}^{*,\beta}_{n_i}}} \subset \left[\widehat{\mathcal{M}^{*,\beta}_{n_j}}\right]_{1/j} \tag{27}$$

for all j.

On the other hand, again by (26), one gets $X \in \left[\widehat{\mathcal{M}^{*,\beta}_{n_i}}\right]_{1/j}$ for all $X \in \widehat{\mathcal{M}^{*,\beta}_{n_j}}$ and $i > j$. Thus, we have that X is in the $1/j$-neighborhood of $\overline{\bigcup_{i>m} \widehat{\mathcal{M}^{*,\beta}_{n_i}}}$. Now, take a point $Y_m \in \overline{\bigcup_{i>m} \widehat{\mathcal{M}^{*,\beta}_{n_i}}}$ so that $d(X, Y_m) < 1/j$ for each $m > j$. We may assume that the sequence $\{Y_m\}$ converges to some Y. This point satisfies $d(X, Y) < 1/j$ and $Y \in \bigcap_{m=0}^{\infty} \overline{\bigcup_{i>m} \widehat{\mathcal{M}^{*,\beta}_{n_i}}}$, so X is in the $1/j$-neighborhood of $\bigcap_{m=0}^{\infty} \overline{\bigcup_{i>m} \widehat{\mathcal{M}^{*,\beta}_{n_i}}}$. Thus, we obtain

$$\left[\bigcap_{m=0}^{\infty} \overline{\bigcup_{n_i>m} \widehat{\mathcal{M}^{*,\beta}_{n_i}}}\right]_{1/j} \supset \widehat{\mathcal{M}^{*,\beta}_{n_j}} \tag{28}$$

for all j. Combining (27) and (28), we complete the proof of the proposition.

2.3. $\mathcal{C}_{\text{Laputa}}$ and J^+

In this section we propose a plausible mathematical definition of Laputa chains according to the numerical observation (iii) and give the proof of the main theorem stated in section 1.

For each final condition $\beta \in \mathbb{R}$, we define

$$\mathcal{M}^{\beta}_{\infty} \equiv \bigcap_{m=0}^{\infty} \overline{\bigcup_{n>m} \mathcal{M}^{*,\beta}_{n}} \tag{29}$$

and

$$\mathcal{M}_{\infty} \equiv \bigcup_{\beta\in\mathbb{R}} \mathcal{M}^{\beta}_{\infty}. \tag{30}$$

Note that the set includes any limit set to which the subsequence $\left\{\widehat{\mathcal{M}^{*,\beta}_{n_i}}\right\}$ converges in the Hausdorff topology, in other words:

$$\lim_{n_i\to\infty} \widehat{\mathcal{M}^{*,\beta}_{n_i}} \subset \widehat{\mathcal{M}^{\beta}_{\infty}}. \tag{31}$$

Thus the candidate for the Laputa chains should exist in it. We supplement our belief with the following fact:

Lemma 2.9. *For any $\beta \in \mathbb{R}$ and any compact set B in $\mathbb{C}^2 \setminus \mathcal{M}_{\infty}$, we have*

$$\sum_{(q,p)\in B\cap\mathcal{M}^{\alpha,\beta}_{n}} A_n(q, p) \exp\left\{\frac{\mathrm{i}}{\hbar} S_n(q, p)\right\} = 0$$

for any sufficiently large n. That is, the complement of $\mathcal{M}_{\infty}$ does not (eventually) contribute to the semiclassical propagator.

Proof. First fix $\beta \in \mathbb{R}$. Then, by the definition of $\widehat{M_{\infty}}$, we have $B \cap \widehat{\mathcal{M}^{\beta}_{\infty}} = \emptyset$. So the distance (the usual distance between two sets, not the Hausdorff distance) between B and

$\widehat{\mathcal{M}^{\beta}_{\infty}}$ is positive. Because $\overline{\bigcup_{n>m}\widehat{\mathcal{M}^{*,\beta}_{n}}}$ is a decreasing sequence of compact sets, we see $B \cap \overline{\bigcup_{n>m}\widehat{\mathcal{M}^{*,\beta}_{n}}} = \emptyset$ for sufficiently large m. Thus, $B \cap \mathcal{M}^{\alpha,\beta}_{n}$ is empty for any large n. □

From proposition 2.7, $\mathcal{M}^{\beta}_{\infty}$ includes the forward Julia set J^{+}. Further, one can prove that $\mathcal{M}^{\beta}_{\infty}$ is included by the forward filled Julia set K^{+}:

Lemma 2.10. *For any $\beta \in \mathbb{R}$ we have $\mathcal{M}^{\beta}_{\infty} \subset K^{+}$.*

Proof. We shall discuss in the (x, y)-plane by the affine change of coordinate $(q, p) = (y - 1, y - x)$. The algebraic set $\mathcal{B}_{\beta}$ is then transformed into another algebraic set which will be denoted by $\mathcal{N}^{\beta}$. By proposition 4.2 of [6], we know the following fact: for any non-zero polynomial $B(x, y)$, there exists n_0 so that $B \circ f^{n_0}(x, y)$ has cy^{k} as the unique term of highest degree. Recall the definition (13) of V^{+}. Choose $R > 0$ sufficiently large and take $(x, y) \in V^{+}$. Then, the absolute value of this highest degree term becomes greater than the absolute value of the remaining term. Thus, one sees that $\mathcal{N}^{\beta} \cap V^{+} = \emptyset$. Let us put $\mathcal{N}^{\beta}_{n} \equiv f^{-n}(\mathcal{N}^{\beta})$. Because $f^{-k}(V^{+})$ is an increasing sequence, we have

$$\bigcup_{n>m} \mathcal{N}^{\beta}_{n} \cap f^{-k}(V^{+}) = \emptyset$$

for any $m \geqslant k \geqslant 0$. Because $\bigcup_{n>m}\mathcal{N}^{\beta}_{n}$ is a decreasing sequence of m, we see

$$\left(\bigcap_{m=0}^{\infty} \overline{\bigcup_{n>m} \mathcal{N}^{\beta}_{n}}\right) \cap \left(\bigcup_{k=0}^{\infty} f^{-k}(V^{+})\right) = \emptyset.$$

One knows that $\bigcup_{k=0}^{\infty} f^{-k}(V^{+})$ coincides with the complement of K^{+} for f. Thus, $\bigcap_{m=0}^{\infty}\overline{\bigcup_{n>m}\mathcal{N}^{\beta}_{n}}$ is contained in K^{+} for f, which is transformed to $\mathcal{M}^{\beta}_{\infty}$ by the affine change of coordinate. Thus, we are done. □

The claims in lemma 2.8 and in the previous lemma are summarized as

Corollary 2.11. *$K^{+} \supset \mathcal{M}^{\beta}_{\infty} \supset J^{+}$ for every $\beta \in \mathbb{R}$. In particular, $K^{+} \supset \mathcal{M}_{\infty} \supset J^{+}$.*

We are interested in the points in $\mathcal{M}_{\infty}$ which contribute to the tunneling phenomena. Note that we have to eliminate the points in $\mathcal{M}_{\infty}$ where $\exp\left\{\frac{1}{\hbar}S_{n}(q, p)\right\}$ diverges or tends to zero. We say that the action Im $S_{n}(q, p)$ *converges absolutely at* (q, p) if

$$\sum_{j=1}^{\infty} |\mathrm{Im}\{H_{0}(p_{j}) + V(q_{j-1}) + q_{j-1}(p_{j} - p_{j-1})\}| < +\infty. \tag{32}$$

The following definition gives a mathematical basis for what we have observed numerically.

Definition 2.12. *We define*

$$\mathcal{C}_{\mathrm{Laputa}} \equiv \{(q, p) \in \mathcal{M}_{\infty} : \mathrm{Im}\ S_{n}(q, p) \text{ converges absolutely at } (q, p)\} \tag{33}$$

and call it the Laputa chain.

Now we present the main results of this section, the proof of the main theorem.

Proof of main theorem (i). Suppose $h_{\mathrm{top}}(g|_{\mathbb{R}^2}) > 0$ and take a saddle point X in $\mathbb{R}^2$. Then, by corollary 2.12, we have $\mathcal{M}_{\infty} \supset J^{+} \supset W^{s}(X)$. On the other hand, every $(q, p) \in W^{s}(X)$

approaches to $\mathbb{R}^2$ exponentially eventually since X is a saddle. Because $H_0(p)$ and $V(q)$ are polynomials, it is not difficult to see that

$$|\mathrm{Im}\{H_0(p_j) + V(q_j) + q_j(p_j - p_{j-1})\}| < C \max\{|\mathrm{Im}\ p_j|, |\mathrm{Im}\ p_{j-1}|, |\mathrm{Im}\ q_j|\},$$

for sufficiently large j, where C denotes a constant depending only on the diameter of J. Thus, Im $S_n(q, p)$ converges absolutely at $(q, p) \in W^s(X)$ and we have $\mathcal{C}_{\mathrm{Laputa}} \supset W^s(X)$. Now the conclusion follows from corollary 2.3.

(ii) This is due to the preceding (i) and theorem 2.3.

(iii) Since we already know that $K^+ \supset \mathcal{M}_\infty \supset \mathcal{C}_{\mathrm{Laputa}}$, it is enough to show $\mathcal{C} \supset J^+$. If g is hyperbolic and $h_{\mathrm{top}}(g|_{\mathbb{R}^2}) = \log 2$, then $J = K \subset \mathbb{R}^2$ by theorem 2.4 and remark 2.5. It then follows that $J^+ = W^s(J) = W^s(J \cap \mathbb{R}^2)$. By the hyperbolicity of J, the orbit of arbitrary point in J^+ converges to $\mathbb{R}^2$ eventually exponentially, so Im $S_n(q, p)$ converges absolutely at this point. Thus, we see that $\mathcal{C}_{\mathrm{Laputa}} \supset J^+$. This completes the proof of our main theorem.

Cases (ii) and (iii) correspond to a specific condition that idealized hyperbolic chaos is realized on J^+, but it should be noted that case (i) covers the most general situations in which the real phase space is a mixture of chaotic and rotational components with KAM circles. The theorem thus claims that it is generic that the intersection of Laputa chains by the initial manifold $\mathcal{A}_\alpha$ is dense in the intersection of the forward Julia set by the initial manifold, $J^+ \cap \mathcal{A}_\alpha$. The forward Julia set J^+ is a large set in the sense of potential theory. Thus, the statement of the main theorem suggests that a bunch of paths in $\mathbb{C}^2$ contributes to the tunneling phenomena if the underlying classical mechanics is chaotic. The high density of the tunneling trajectories in the chaotic case is quite different from the integrable systems[5] where only a sparse set of instanton solutions contributes to the propagator.

Remark 2.13. It can be shown that $\mathcal{C}_{\mathrm{Laputa}} \neq J^+$ when $h_{\mathrm{top}}(g|_{\mathbb{R}^2}) < \log 2$. To see this, we first recall that the saddle periodic points are dense in J when f is hyperbolic [6]. Thus, by theorem 2.4 and remark 2.5, there is a saddle $p \in J$ outside $\mathbb{R}^2$ when $h_{\mathrm{top}}(g|_{\mathbb{R}^2}) < \log 2$. The points in the stable manifold of this saddle belong to J^+ but not to $\mathcal{C}_{\mathrm{Laputa}}$. The main theorem, however, asserts that arbitrarily close to such an 'undesired' point there always exist points belonging to $\mathcal{C}_{\mathrm{Laputa}}$.

We have so far discussed the nature of tunneling trajectories on the entrance side. However, applying the same arguments as before to the forward evolution process, we obtain an important characterization of the tunneling trajectories on the exit side. Let us consider the set $\mathcal{L}_n^{\alpha,\beta} = g^n\big(\mathcal{M}_n^{\alpha,\beta}\big)$ defined by equation (11). It is the counterpart of $\mathcal{M}_n^{\alpha,\beta}$ on the exit side and thus forms the support of the semiclassical wavefunction. Corresponding to the set $\mathcal{M}_\infty^\beta$ defined by equation (29), we introduce the set

$$\mathcal{L}_\infty^\alpha \equiv \bigcap_{m=0}^{\infty} \overline{\bigcup_{n>m} \mathcal{L}_n^{\alpha,*}} \qquad \text{where} \qquad \mathcal{L}_n^{\alpha,*} = \{(q_n, p_n) \in \mathbb{C}^2 : A(q, p) = \alpha\}. \tag{34}$$

Then following the same argument used to deduce corollary 2.11, its exit version immediately follows.

Corollary 2.14. *$K^- \supset \mathcal{L}_\infty^\alpha \supset J^-$ for every $\alpha \in \mathbb{R}$.*

If the intersection of $\mathcal{L}_\infty^\alpha$ by the final manifold $\mathcal{B}_\beta$ is taken, corollary 2.14 claims the nature of the converging components in the set $\mathcal{L}_n^{\alpha,\beta}$, that is, the set of endpoints of tunneling trajectories defined by equation (11). On the other hand, according to the numerical observation (i), the

[5] The continuous flow system with the cubic potential is a typical example.

endpoints of dominantly contributing trajectories, which are launched from the trunk part of Laputa chains, land in the real plane in the limit $n \to \infty$. We therefore make the following conjecture.

Conjecture 2.15. *The trajectories from the trunk part of the Laputa chains land on* $\mathcal{L}^{\alpha}_{\infty} \cap \mathbb{R}^2$ *in the limit of* $n \to \infty$.

Thus the support of semiclassical wavefunction contributed by the trunk part of the Laputa chains is bounded by $J^- \cap \mathbb{R}^2$ and $K^- \cap \mathbb{R}^2$ from below and above, respectively. The above characterization of the tunneling trajectories on the exit side will be re-examined numerically in the following section.

3. Physical implications of the mathematical theorems

In this section, we examine the physical significance of mathematical claims presented in the previous section, by comparing them with numerical results. As a particular physical system, we take the parameter of the cubic potential a (see equations (3) and (4)) a positive real number, and identify the quadratic map g with the Hénon map f where no confusion arises.

We focus on the two sets

$$\mathcal{M}^{\alpha}_{n} = \bigcup_{\beta \in \mathbb{R}} \mathcal{M}^{\alpha,\beta}_{n}, \qquad \mathcal{L}^{\alpha}_{n} = \bigcup_{\beta \in \mathbb{R}} \mathcal{L}^{\alpha,\beta}_{n}. \tag{35}$$

These sets were used in part I to represent tunneling trajectories at the entrance and exit sides, respectively. We also focus on the trunk parts of Laputa chains, hereafter denoted by $\mathcal{C}^{\alpha}_{n}$. We will examine how the asymptotic behavior of the trunk part of Laputa chains is consistent with our main theorem.

In the next two subsections we first consider ideal situations corresponding respectively to the cases (iii) and (ii) in the main theorem. These cases both represent idealized limits of chaotic dynamics and they form the basis for understanding more realistic situations. The two claims (ii) $\overline{\mathcal{C}_{\text{Laputa}}} = J^+$ and (iii) $\mathcal{C}_{\text{Laputa}} = J^+$ in the main theorem are similar in the sense that they both assert that the Julia set is a good approximation to the Laputa chain. But as will be explained below, there is a crucial difference, which is a manifestation of what is mentioned in remark 2.13.

3.1. Real horseshoe case: an ideal model for the Laputa chain

It is well known that the Hénon map has the real component of K^+ when the nonlinearity parameter a is positively large. In this subsection we confine ourselves to the case where the condition for the claim (iii) is realized. If f is hyperbolic and $h_{\text{top}}(f|_{\mathbb{R}^2}) = \log 2$, $K = J \subset \mathbb{R}^2$ follows from theorems 2.3 and 2.4. Under these conditions, the Hénon map f satisfies the horseshoe condition: there exists a continuous semi-conjugacy onto the two-shift on $J \subset \mathbb{R}^2$ and every trajectory on J has its own infinite binary symbol sequence both in forward and backward directions. It was proved that the Hénon map is hyperbolic and conjugate to the two-shift if $a > a_c$, where a_c denotes the first tangency parameter [12]. a_c is numerically evaluated in [13] as $a_c = 5.6993\ldots$.

In the ideal cases, some considerations must be taken for the choice of the initial manifold so that the transition to the chaotic region may occur *only* by the tunneling trajectories. This can be achieved by recalling the filtration property of the Hénon map. From equation (14), the filled Julia set $K = K^+ \cap K^-$, which contains the Julia set J, is in $V^+ \cap V^-$. We choose $\mathcal{A}_{\alpha}$ such that $g(\mathcal{A}_{\alpha} \cap \mathbb{R}^2) \subset V^+$. Then, because $g^n(V^+) \subset V^+$ for $n > 0$, no trajectories from the

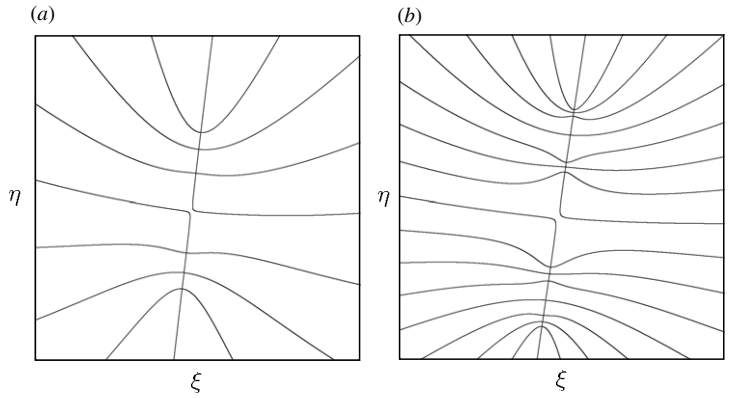

Figure 1. Typical examples of the set $\mathcal{M}_n^\alpha$ in the horseshoe parameter region ($a = 8$), where (*a*) $n = 7$ and (*b*) $n = 8$. See also figures 4 and 6 in part I.

real component of $\mathcal{A}_\alpha$ fall into the region $V^+ \cap V^- \supset J$, which means that classical transition into the chaotic region is forbidden.

In the present and the next subsections we take the following initial and final manifolds $\mathcal{A}_\alpha = \{(q, p);\ p = \alpha\}$ and $\mathcal{B}_\beta = \{(q, p);\ p = \beta\}$, respectively, as defined by equation (22). For this choice of $\mathcal{A}_\alpha$, the above condition is realized by taking α sufficiently less than $-\sqrt{|c|} = -\sqrt{|1-a|}$.

The set $\mathcal{M}_n^\alpha$ for such a choice of $\mathcal{A}_\alpha$ is shown in figure 1. A sequence of branches is aligned in the vertical direction in the (ξ, η)-plane. This reflects the fact that $K^+ \cap \mathcal{A}_\alpha$ is also aligned vertically to the real axis. Caustics are located between every pair of branches (not shown in the figure). This chained object can be regarded as the most idealized model of the Laputa chain. As discussed in section 3.2 of part I, the main part of the chain is called the *trunk*, which has a feature that the trajectories launched at the trunk part approach rapidly the real plane.

As was discussed in section 3.1 of part I, the branches which do not form chained objects coexist with the Laputa chains in non-hyperbolic cases where rotation domains coexist with hyperbolic components. However, in the real horseshoe case, that is g is hyperbolic in the real phase space, where there exist no rotation domains, all the branches belong to a Laputa chain.

In order to see how the claim (iii) in the theorem is realized in the initial value plane, we here focus on how the set $\mathcal{M}_n^\alpha$ behaves with n. As shown in figure 1, every branch in the Laputa trunk chain in the horseshoe case bifurcates into two branches within a single iteration. Such a doubling of branches occurs in every step and so the number of branches increases as 2^n.

Now we consider the slice of the stable manifold $W^s(R)$ (locally complex-1D manifold in $\mathbb{C}^2$) by the initial manifold $\mathcal{A}_\alpha$ (complex-1D curve in $\mathbb{C}^2$). Here R denotes an unstable periodic point (simply called a saddle or a periodic saddle hereafter) in the real plane. As $W^s(R)$ is folded infinitely many times and so is entangled with $\mathcal{A}_\alpha$ to form infinite number of intersection points. Among them, we specifically consider the *primary intersection* of $W^s(R)$. The primary intersection is defined as an intersection point at which the stable manifold $W^s(R)$ emanating from a saddle R of period n *first* intersects with $\mathcal{A}_\alpha$.

More precisely, we define the primary intersection as follows. Recall that there is a conjugation map Φ from $\mathbb{C}$ to $W^s(R)$ such that

$$\Phi^{-1} g^n \Phi = g_{sn} \quad \text{where} \quad g_{sn}(\zeta) = \lambda^{-1}\zeta \tag{36}$$

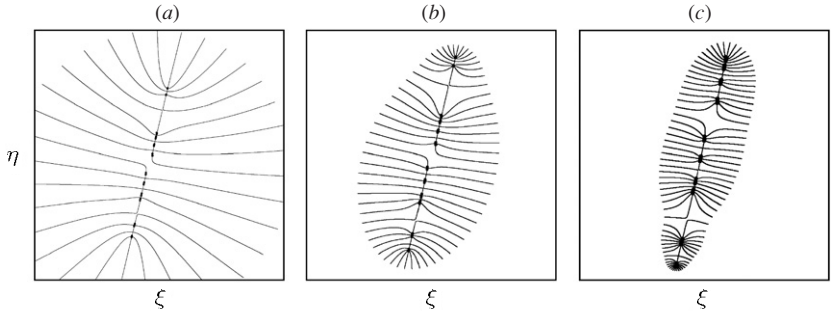

Figure 2. The Laputa chain and primary intersections of $W^s(R)$ and $\mathcal{A}_\alpha$ (dots). (*a*) $n = 8$, (*b*) $n = 9$ and (*c*) $n = 10$. In order to see the shrinking objects clearly, (*b*) is magnified 1.3 times and (*c*) 2.0 times as compared to (*a*).

for $\zeta \in \mathbb{C}$ [22]. Here λ denotes the larger eigenvalue of the tangent map of g^n at R. The coordinate ζ is normalized so that the map g^n is expressed by a linear transformation. By the primary intersection we mean the intersection with the smallest $|\zeta|$. A period n orbit is composed of n points, and so we have n primary intersections corresponding to each component.

In the horseshoe regime, all the periodic saddles are on $\mathbb{R}^2$ and each saddle with period n is coded by n binary symbols. If we distinguish all the points composing a single periodic orbit, 2^n saddle points of cycle n are located on the set J and each has $W^s(R)$ extended in the complex domain. As will be discussed closely in [14], the primary intersection points of 2^n stable manifolds $W^s(R)$ with $\mathcal{A}_\alpha$ have one-to-one correspondence to the 2^n bifurcated branches forming the Laputa trunk at the nth step. In fact each of 2^n intersection points is located close to the trunk part of one of the 2^n branches, and so each branch is assigned to n binary symbols.

We give a further remark. Corollary 2.2 claiming that $\overline{W^s(X)} = J^+$ implies that $\mathcal{C}_{\text{Laputa}} \cap \mathcal{A}_\alpha$ is approximated well by the intersections of W^s of only a single arbitrarily chosen saddle X and $\mathcal{A}_\alpha$. If all the higher order intersections coming from *only a single saddle* are plotted, they mimic the distribution of the primary intersection points.

In figure 2, the set $\mathcal{M}_n^\alpha$ from $n = 8$ to $n = 10$ is presented. Here the final momentum β specifying the final manifold $\mathcal{B}_\beta$ is not scanned from $-\infty$ to ∞ but is confined in a bounded range $|\beta| < B$ (B is taken large enough but finite) according to the order of the asymptotic limits taken in deriving the main theorem, namely first taking $n \to \infty$ with fixed β and next allowing β to be unbounded. (We extract the trunk parts $\mathcal{C}_n^\alpha$ by the empirical criterion introduced in section 4.2 in part I together with the condition $|\beta| < B$.)

Evidently, the trunk part along each of the 2^n branches, which were formed as a result of successive splitting, shrinks exponentially to the intersection of $W^s(R)$ with increase of n. As $n \to \infty$, the Laputa chain converges to a set composed of an infinite number of points, to each of which a semi-infinite series of binary symbols can be assigned. This observation means that the Laputa chain $\mathcal{C}_n^\alpha$ converges to $J^+ \cap \mathcal{A}_\alpha$, which is just the claim of the main theorem $\mathcal{C}_{\text{Laputa}} = J^+$.

Finally, we discuss how the trunk part manifests itself in the tunneling component of the wavefunction on its support $\mathcal{L}_n^\alpha \big(= g^n\big(\mathcal{M}_n^\alpha\big)\big)$. Let the trunk part assigned to a saddle R be $\mathcal{C}_n^\alpha(R)$. If the formal limit $n \to \infty$ is taken, the trunk is on the intersection of $J^+ \cap \mathcal{A}_\alpha$. However, if n is large but finite, $\mathcal{C}_n^\alpha(R)$ is very close to the intersection but is not exactly on it. The trajectories from the trunk are first guided by $W^s(R)$ and pass close to the saddle R,

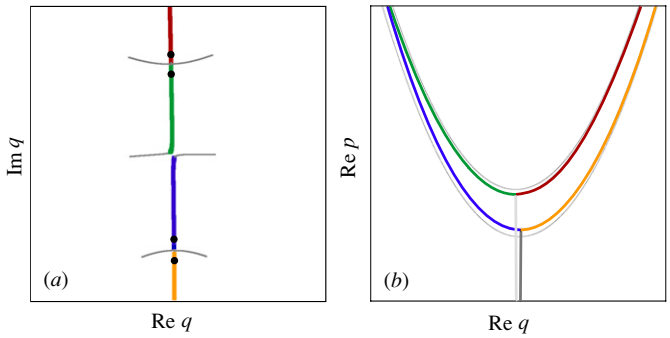

Figure 3. (*a*) The Laputa chain $\cup_{|\beta|<B}\mathcal{M}_n^{\alpha,\beta}$ with $n = 5, a = 6, \alpha = -15$ and $B = 20$. The dots represent the intersection $W^s(R) \cap \mathcal{A}_\alpha$. (*b*) The final set $\cup_{|\beta|<B}\mathcal{L}_n^{\alpha,\beta}$ projected onto (Re q_n, Re p_n) plane and the unstable manifold for a fixed saddle. The unstable manifold is composed of infinitely many folded curves and one of them is indistinguishable from this final set. The colors in (*b*) correspond to the colors in (*a*). (These figures are taken from [5] with permission.)

and then they are stretched along $W^u(R)$. They finally end in vicinities exponentially close to $W^u(R)$ [14].

Since the boundary condition Im $p_n = 0$ is imposed, the transported set $g^n\left(\mathcal{C}_n^\alpha(R)\right)$, which is a subset of $\mathcal{L}_n^\alpha$, is very close to $W^u(R) \cap \mathbb{R}$. On the other hand, Im q_n converges to 0 as $n \to \infty$, they will be on $W^u(R) \cap \mathbb{R}^2$ in the limit $n \to \infty$. As demonstrated in figure 3, the final set $\cup_{|\beta|<B}\mathcal{L}_n^{\alpha,\beta}$ is almost indistinguishable from a part of the unstable manifold, implying that not only Im $p_n = 0$ but also Im q_n is small enough. Since $J^- = \overline{W^u(R)}$, this is what is mentioned in conjecture 2.15

Recall the relation $\partial S_n(\alpha, \beta)/\partial\beta = -q_n$ for the classical action (7), then $|\text{Im } S_n(\alpha, \beta)/\partial\beta| = |\text{Im } q_n|$ is very small along the set $g^n\left(\mathcal{C}_n^\alpha(R)\right)$, which means that Im $S_n(\alpha, \beta) = \int \mathrm{d}\beta\, \text{Im } q_n(\beta)$ keeps almost the same value along $g^n\left(\mathcal{C}_n^\alpha(R)\right) \sim W^u(R) \cap \mathbb{R}^2$, and the wavefunction forms a plateau along the real unstable manifold $W^u(R)$ extended far beyond the attractive region of the cubic potential. This is just what the numerical observation (i) describes.

3.2. Complex hyperbolic case

In this subsection we examine the case where g is hyperbolic on $K = J$, but J is not contained in $\mathbb{R}^2$. Once the first tangency occurs at $a = a_c$, the real horseshoe is broken [12] and some parts of J fall into the complex domain. The topological entropy $h_{\text{top}}(g|_{\mathbb{R}^2})$ becomes less than $\log 2$. However, it has been proved that there certainly exist such parameter loci in which the Hénon map is hyperbolic and so J^+ and J^- intersect transversally in $\mathbb{C}^2$ even in case $a < a_c$ [15, 16].

3.2.1. Multi-generation structure. We first demonstrate how the destruction of the real horseshoe manifests itself in the structure of $\mathcal{M}_n^\alpha$. Recall that, just before the first tangency, the intersections of $\mathcal{A}_\alpha \cap K^+ = \mathcal{A}_\alpha \cap J^+$ are aligned along a line almost vertical to the real axis of the (ξ, η)-plane as shown in the previous subsection. We here consider what happens after the first tangency. If the saddle-node type bifurcation occurs for example, a pair of real saddles, say R and R', degenerates and moves into the complex plane, forming complex conjugate saddles. Correspondingly, the *primary* intersections in $W^s(R) \cap \mathcal{A}_\alpha$ and $W^s(R') \cap \mathcal{A}_\alpha$ come

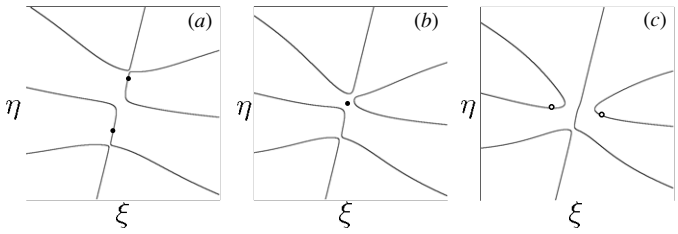

Figure 4. Bifurcation of primary intersections $W^s(R) \cap \mathcal{A}_\alpha$ and $W^s(R') \cap \mathcal{A}_\alpha$ and the corresponding Laputa branches. The filled circles and open circles denote primary intersections for real saddles and those for complex saddles, respectively. The parameters are given as $n = 8, \alpha = -15$, and (*a*) $a = 5.0$, (*b*) $a = 4.86$ and (*c*) $a = 4.80$.

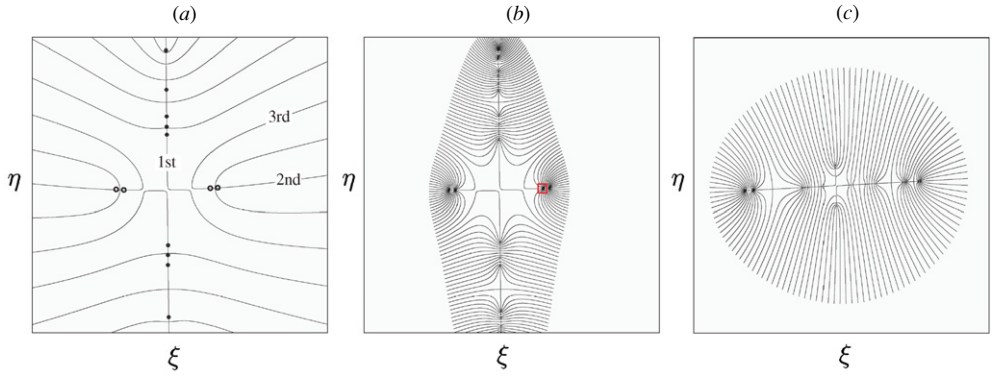

Figure 5. A Laputa chain accompanied by side chains observed in the complex hyperbolic case ($a = 5.3$) at (*a*) $n = 14$, (*b*) $n = 17$ and (*c*) $n = 20$, where (*c*) is a magnification of a small red box in (*b*). In (*a*), the filled and open circles indicate intersections of the initial manifold $\mathcal{A}_\alpha$ with W^s of real saddles and of complex saddles, respectively.

closer to each other along the vertical line, degenerate, and next bifurcate to form a pair aligned in the direction perpendicular to the vertical line, as is shown in figure 4.

Our main theorem implies that the Laputa branches, which are aligned to form a single trunk along the vertically lined intersections $\mathcal{A}_\alpha \cap J^+$ in the horseshoe limit, should also reform in accordance with the rearrangement of $\mathcal{A}_\alpha \cap J^+$.

Indeed, the Laputa branches also move off from the aligned trunk chain and form side branches in the direction perpendicular to the trunk chain. Numerical results show that for sufficiently large n the side branches are split into new branches to form the *side chain* as shown in figure 5. Note that, as is expected from the main theorem, the intersections $\mathcal{A}_\alpha \cap W^s(X)$ are located close to each of the branches forming the side chain.

Formation of side chains does not terminate only at the first stage. With increase of n, side chains of new generation are further generated from the older side chains. In the limit of $n \to \infty$ the whole set $\mathcal{M}_n^\alpha$ eventually forms a tree structure composed of a hierarchy of chains as is demonstrated in figure 5. The trunk chain is referred to as the first generation of the hierarchy, and side chains extending perpendicularly to the trunk as the second one, and the one extending perpendicularly to the second generation as the third one and so on. We call such a hierarchical structure formed in $\mathcal{M}_n^\alpha$ *multi-generation structure* hereafter. This is a general feature asserted in numerical observation (ii). (See also section 4.1 of part I.)

Each side chain has its own trunk part, whose trajectories finally approach the real plane. However, the itinerance of the trajectories from side chains has a characteristic feature different

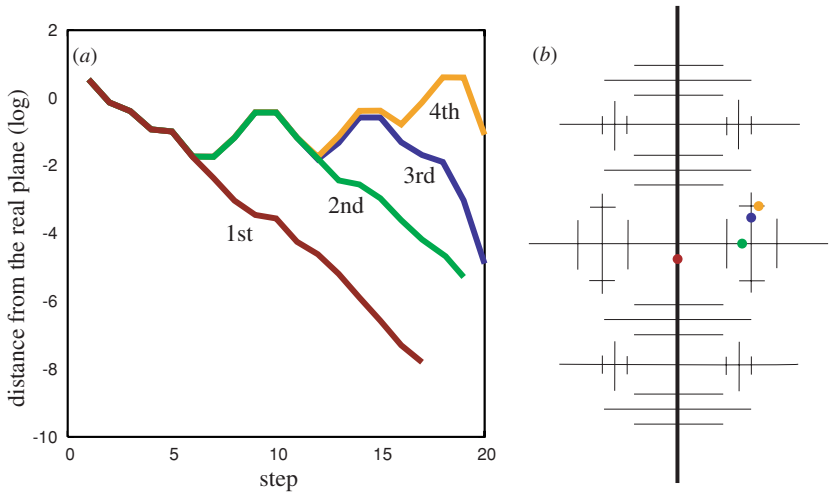

Figure 6. Typical behaviors of trajectories starting at side chains of first, second, third and fourth generations. Nonlinearity parameter $a = 5.3$. (a) The distance between the trajectory and the real plane (in log scale), and (b) the corresponding initial conditions in the (ξ, η)-plane (schematic).

from the first-order trajectories. It is interesting to note that multi-generation structure similar to the present case was observed in another map model (called the scattering map model) describing the barrier tunneling process [3]. In particular, in the scattering map model, with the aid of a kind of symbolic coding assigned to the tree structure, a more precise specification of the multi-generation structure is possible [3].

Without precise knowledge about the bifurcation process of complex saddles we cannot establish a complete scenario for the development of the multi-generation structure. This is linked to a variety of combinations of bifurcations, for which general theory is difficult to be developed, and so we will not pursue this issue further. Instead, we discuss in the following subsection how the multi-generation structure plays roles in the tunneling problem. A new family of trajectories showing an itinerary not appearing in the horseshoe regime comes in there.

3.2.2. Tunneling trajectories itinerating in complex space. As mentioned before, it is a common feature that trajectories starting from the trunk of side chains finally approach the real plane. But the approach is not monotonic, rather the trajectories sometimes wander in complex space and approach exponentially in the final stage.

In figure 6, we show the behavior of typical trajectories launched at side chains of different generations. We can see that as the generation advances the time spent wandering in complex phase space becomes longer. In addition, we note a simple rule in their behavior: a trajectory starting at a side chain of higher generation behaves similar to the trajectory of lower order generation for a certain initial time period.

Here we explain that the existence of wandering trajectories together with the appearance of side branches of higher order generation can be understood by combining the statement $\overline{W^s(X)} = J^+$ and the main theorem.

An important property which is expected from the claim (ii) of the main theorem and corollary 2.2, is that a branch in a Laputa chain exists close to an intersection of $\mathcal{A}_\alpha$ and $W^s(R)$ if the time step n is taken sufficiently large. Let R_i and C_j be periodic saddles in the real and

complex planes, respectively. Let the primary intersections between $\mathcal{A}_\alpha$ and W^s of real and complex saddles be denoted by $P_i(\in W^s(R_i) \cap \mathcal{A}_\alpha)$ and $Q_i(\in W^s(C_i) \cap \mathcal{A}_\alpha)$, respectively.

Consider a side branch in the second generation, which lies close to the intersection point denoted by $Q_1 = W^s(C_1) \cap \mathcal{A}_\alpha$. Since Q_1 is close to P_1 (see figure 5(*a*)), the trajectories starting at P_1 and Q_1 follow similar itineraries in the initial time stage. But the trajectory launched at Q_1 eventually approaches C_1 by definition and cannot reach the real plane. However, the property $\overline{W^s(X)} = J^+$ (corollary 2.2) implies that in a very close neighborhood of Q_1 there exists an intersection $P_2' \in W^s(R_2) \cap \mathcal{A}_\alpha$ of a real saddle R_2 (R_2 can be R_1). Let the primary intersection of $W^s(R_2)$ and $\mathcal{A}_\alpha$ be P_2, then the trajectory from P_2 goes directly toward R_2, whereas the trajectory from P_2' first approaches C_1 because P_2' is very close to $Q_1 = W^s(C_1) \cap \mathcal{A}_\alpha$ then goes toward R_2, which means that P_2' is a secondary intersection of $W^s(R_2)$ with $\mathcal{A}_\alpha$. In other words, the trajectory from P_2' makes a side trip in the complex domain before going toward the real plane. In the final stage toward R_2, it stays close to the trajectory from P_2. According to the main theorem, if the step n is taken larger, a branch appears close to a secondary intersection P_2'. Other saddles in the real plane also contribute to the branches, which are observed as the side chain of the second-order generation.

In the same way, there exists $Q_2' = W^s(C_2) \cap \mathcal{A}_\alpha$ which is located just at the side of P_2', where C_2 denotes another complex saddle. Then Q_2' plays the role of a seed germinating the tertiary intersection. The side chain of the third order appears very close to the tertiary intersection P_3'' of the intersection $\mathcal{A}_\alpha \cap W^s(R_3)$, if n is large enough. Inductively, the mth-order generation germinates from the $(m-1)$ th-order generation.

The itineraries of the orbits launched at a series of higher order intersections as well as the corresponding higher order generation side chains are as follows:

$$\begin{aligned}
&\text{1st-generation} \quad P_1 \Rightarrow R_1 \\
&\text{2nd-generation} \quad P_2' \Rightarrow R_1 \Rightarrow C_1 \Rightarrow R_2 \\
&\text{3rd- generation} \quad P_3'' \Rightarrow R_1 \Rightarrow C_1 \Rightarrow R_2 \Rightarrow C_2 \Rightarrow R_3 \\
&\text{4th-generation} \quad P_4''' \Rightarrow R_1 \Rightarrow C_1 \Rightarrow R_2 \Rightarrow C_2 \Rightarrow R_3 \Rightarrow C_3 \Rightarrow R_4 \\
&\cdots\cdots\cdots\cdots\cdots\cdots\cdots\cdots
\end{aligned} \tag{37}$$

By the definition of the Laputa chain, the trajectory from it must approach the real plane in the final stage, while the final approach to the real plane is delayed as the generation becomes higher. Therefore, the generation number of the observed side chain in the (ξ, η)-plane becomes higher. This is what we have observed in the set $\mathcal{M}_n^\alpha$ numerically.

The above scenario is supported by the main theorem and corollary 2.2. However, this scenario is not rigorous in a mathematical sense. To make this rigorous we need the next theorem which can be derived from the potential theory.

Theorem 3.1 (Bedford–Lyubich–Smillie [9]). *Let X and X' be two saddles of g. Then, the set of transverse intersections of $W^s(X)$ and $W^u(X')$ is dense in the support of μ.*

Now, the following gives a mathematical statement about the existence of initial set on $W^s(R_i)$ whose trajectories exhibit chaotic itinerance among the complex saddles.

Theorem 3.2. *Let $0 < h_{\mathrm{top}}(g|_{\mathbb{R}^2}) < \log 2$ and let C_i $(1 \leqslant i \leqslant N)$ and R be saddle periodic points in $\mathbb{C}^2 \setminus \mathbb{R}^2$ and a real saddle periodic point, respectively. Take any positive integers k_i and arbitrary neighborhood U_i of C_i $(1 \leqslant i \leqslant N)$. Then, there exists a point $P \in W^s(R)$ in $\mathbb{C}^2 \setminus \mathbb{R}^2$ such that its orbit stays in U_i at least k_i-times iterates.*

Proof. We first remark that there are saddle points in $\mathbb{C}^2 \setminus \mathbb{R}^2$ because $h_{\mathrm{top}}(g|_{\mathbb{R}^2}) < \log 2$. Because $h_{\mathrm{top}}(g|_{\mathbb{R}^2}) > 0$, there exists a saddle R in $\mathbb{R}^2$ by Katok theorem [10].

Consider the two saddles R and C_1. By theorem 3.1 $W^u(C_N)$ and $W^s(R)$ have a transverse intersection w_N. If we take a sufficiently small neighborhood V_N of w_N in $W^s(R)$, then the backward orbit $g^{-n}(V_N)$ $(n \geqslant 0)$ is contained in U_N for at least k_N-times iterates. Moreover, $g^{-n}(V_N)$ becomes close to $W^s(C_N)$ for large n by Lambda lemma.

Next we consider C_N and C_{N-1}. Because $W^u(C_{N-1})$ and $W^s(C_N)$ have a transverse intersection, $W^u(C_{N-1})$ and $g^{-n}(V_N)$ also have transverse intersection w_{N-1}. If we take a sufficiently small neighborhood V_{N-1} of w_{N-1} in $g^{-n}(V_N)$, then the backward orbit $g^{-n}(V_{N-1})$ $(n \geqslant 0)$ is contained in U_{N-1} for at least k_{N-1}-times iterates.

By repeating this procedure, we obtain a disc $V_1 \subset W^s(R)$. Then, the orbit of a point $z \in g^{-n}(V_1) \in W^s(R)$ for a sufficiently large n satisfies the requirements in the theorem. Thus, we are done.

Since we focus on the wandering trajectory in $\mathbb{C}^2$, all C_i are supposed to be in $\mathbb{C}^2 \setminus \mathbb{R}^2$ in the above theorem, but the above proof is valid even if C_i is a real saddle. Then the wandering trajectory mentioned in the theorem has the itinerary of (37). We stress that the above theorem is not restricted to the hyperbolic case. □

3.2.3. Contribution of complex chaotic trajectories to tunneling. We have described a novel class of tunneling trajectories which exhibit erratic wandering in complex phase space. We here discuss whether or not such complex trajectories actually contribute to the tunneling probability.

To this end, we recall how the tunneling wavefunction is reproduced by the chained branches forming the first-order generation. In the horseshoe case, for every real saddle R_i there exists a primary intersection P_i between $W^s(R_i)$ and $\mathcal{A}_\alpha$. In the vicinity of P_i the branches of the first-order chain exist and the trajectories from them directly approach R_i and land close to $W^u(R_i) \cap \mathbb{R}^2$ as was explained in subsection 3.1. Thus the imaginary part of the action is well approximated by Im $S_{n=\infty}(P_i)(> 0)$, where $S_{n=\infty}(P_i)$ is the action defined by equation (7) along the trajectory from the primary intersection P_i. The tunneling tail is extended along every $W^u(R_i) \cap \mathbb{R}^2$ with magnitude $\sim \mathrm{e}^{-\mathrm{Im}\ S_{n=\infty}(P_i)/\hbar}$ in the limit of $n \to \infty$. Since $\overline{W^u(R_i)} = J^-$, many components of the tunneling wavefunction along the real unstable manifolds $W^u(R_i) \cap \mathbb{R}^2$ are supported by the set $J^- \cap \mathbb{R}^2$. These many components are superposed and the probability is roughly estimated by $\mathrm{e}^{-\min_i\{\mathrm{Im}\ S_{n=\infty}(P_i)\}/\hbar}$.

We here assume that there exists a single chaotic component in the real plane. There appears one Laputa chain associated with it and a hierarchy of side chains also follows. An important fact in the present case is that J^- is *not disconnected* in the real phase plane, and the trajectories coming from higher order side chain and the first-order chain finally land along the connected $J^- \cap \mathbb{R}^2$.

The trajectories from each side chain of Nth generation exhibit itineraries as in (37). On the way to R_N, the trajectories first approach R_1 and next wander over the real saddles $R_1, R_2, \ldots$, and the complex saddles $C_1, C_2, \ldots$. Then the imaginary part of the action along the trajectory, which we denote by Im S'_n, is the sum of Im $S_{n=\infty}(P_1)$ and some additional part gained in the late itinerary wandering over R_j s and C_j s. So we can expect Im $S'_n >$ Im $S_{n=\infty}(P_1)$ in general. The trajectories finally land very close to the real unstable manifold of R_N, namely, $W^u(R_N) \cap \mathbb{R}^2$, which is well approximated by $J^- \cap \mathbb{R}^2$. However, along $J^- \cap \mathbb{R}^2$ the trajectories from the first-order chain also land and their contribution exceeds the contributions by higher order side chains as

$$\mathrm{e}^{-\mathrm{Im}\ S'_n/\hbar} < \mathrm{e}^{-\mathrm{Im}\ S_{n=\infty}(P_1)/\hbar} \leqslant \mathrm{e}^{-\min_i\{\mathrm{Im}\ S_{n=\infty}(P_i)\}/\hbar}. \tag{38}$$

Consequently, we may expect that the contribution by the complex chaos cannot be observed in this situation. This is illustrated in figure 7(*a*).

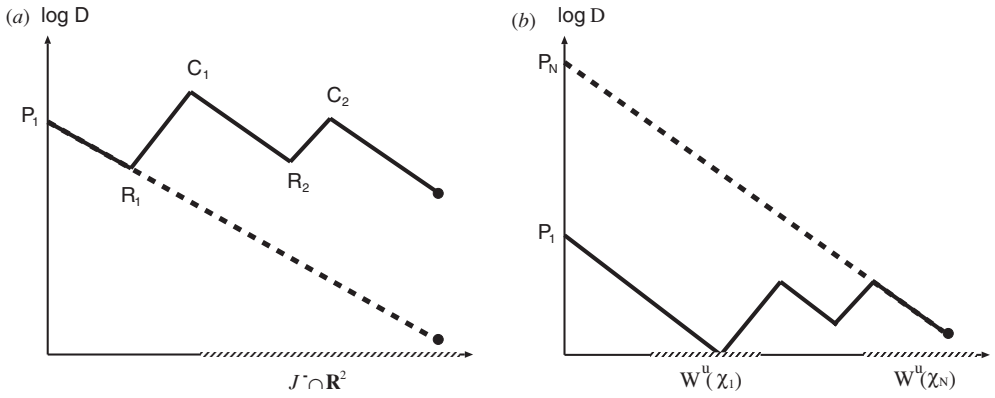

Figure 7. A schematic illustration of (*a*) non-contributing and (*b*) contributing complex-chaotic trajectories. The solid and broken lines indicate a complex-chaotic trajectory and a complex trajectory directly approaching to the real plane, respectively. D is the distance of the trajectory from the real phase plane. See the text for details.

However, this is not the actual case. After the first tangency, there appear more than one invariant set in the real plane, each of which has a positive topological entropy. Such situations can occur even in the case where the system is hyperbolic [15, 16], but more physically important is the case of mixed phase space, in which different chaotic invariant sets are disconnected. Correspondingly, there emerge many first-order Laputa chains whose origins are different chaotic components.

As a decreases further from a_c, many chaotic components with comparable scales which are mutually separated by KAM circles appear in the real plane. This of course is typical for mixed phase space. In such a situation, the contribution from the side chain may become significant, that is observable, for the following reason.

Let the disconnected chaotic components in the real plane be $\mathcal{X}_1, \mathcal{X}_2, \ldots$. Each $\mathcal{X}_i$ contributes to the corresponding chain of the first generation on different sites of $\mathcal{A}_\alpha$, in other words, every set $\mathcal{X}_i$ has its own first-order chain. The trajectories from the branches of each first-order chain approach $\mathcal{X}_i$ on $\mathbb{R}^2$, and they end along the real component of the unstable sets $W^u(\mathcal{X}_i) \cap \mathbb{R}^2$. They are separated from each other and each of them is approximately a subset of $J^- \cap \mathbb{R}^2$. Let Im $S_{n=\infty}(i)$ be a representative value of the imaginary part of the action along the trajectories going toward the saddles in $\mathcal{X}_i$. Then the contribution by the first-order chain to the tunneling tail, supported by $W^u(\mathcal{X}_i) \cap \mathbb{R}^2$, is evaluated as $\mathrm{e}^{-\mathrm{Im}\ S_{n=\infty}(i)/\hbar}$. Every first-order chain has side chains whose trajectories follow the itinerary described by the scheme (37). Such trajectories are first attracted by $R_1 (\in \mathcal{X}_1)$, and finally land along $W^u(\mathcal{X}_N) \cap \mathbb{R}^2$. As discussed above, their imaginary action is Im $S_{n=\infty}(1)$ plus something gained through the itinerary around the real saddles and the complex saddles.

If we suppose that $\mathcal{X}_i$s are separated in the real plane, then |Im $S_{n=\infty}(i)$|'s may take significantly different values. It may happen that

$$|\mathrm{Im}\ S_{n=\infty}(1)| \ll |\mathrm{Im}\ S_{n=\infty}(N)|. \tag{39}$$

Then the imaginary part of the action along the trajectory, denoted by Im S'_n, may be still less than Im $S_{n=\infty}(N)$, which determines the contribution from the first-order chain of $\mathcal{X}_N$. In this case, as is illustrated in figure 7(*b*), among the contributors to the tunneling tail supported by $W^u(\mathcal{X}_N) \cap \mathbb{R}^2$, the contribution from the higher order side chains is larger than that from the

first-order chain associated with $\mathcal{X}_N$ as

$$\mathrm{Im}\, e^{-S'_n/\hbar} > \mathrm{Im}\, e^{-S_{n=\infty}(N)/\hbar}. \tag{40}$$

Then the trajectories for higher order generations could contribute significantly, i.e., make a dominating contribution, to the tunneling probability [17]. We indeed encounter such an example in the following subsection.

3.3. Non-hyperbolic case: existence of rotation domain

In this subsection, we examine the situation in which the dynamical tunneling in the ordinary sense is observed. In particular, we examine the consequence of the existence of rotation domains. It is of particular importance that the claim (i) in the main theorem holds even if KAM curves and chaotic seas coexist in the real phase space. Here we consider the case where a rotation domain develops around the period-1 elliptic point, denoted by $E = (-\sqrt{a}, 0)$, at the bottom of the cubic potential defined in equation (4). This elliptic point is stable if $0 < a < 4$.

Recall the assertion (iii) of the main theorem: the closure of Laputa chain $\mathcal{C}_{\mathrm{Laputa}}$ is bounded by J^+ and K^+ from below and above, respectively. Before going into the main subject of this subsection, we propose a conjecture relating J^+ and K^+, from which the close connection between $\mathcal{C}_{\mathrm{Laputa}}$ and J^+ claimed in the hyperbolic case can be extended in the non-hyperbolic case. The conjecture, which we call the vacant interior conjecture, is as follows:

Conjecture 3.3 (vacant interior conjecture). *The filled Julia sets of the area-preserving Hénon map have no interior points:*

$$J^{\pm} = K^{\pm}, \qquad \text{hence } J = K. \tag{41}$$

We provide in appendix A numerical evidence strongly supporting this conjecture together with some mathematical reasonings. If this is indeed the case, the most general statement in the main theorem, claim (i), becomes a stronger assertion:

$$\overline{\mathcal{C}_{\mathrm{Laputa}}} = J^+. \tag{42}$$

Therefore, if the vacant interior conjecture is true, the same relation as the hyperbolic case holds even in the non-hyperbolic case.

3.3.1. Laputa chains and J^+. If the vacant interior conjecture is true, equation (42) tells that the Laputa chain closely links to J^+ and also to the stable manifold of any saddle by corollary 2.2 as in the ideal hyperbolic case, even if the system is non-hyperbolic and rotation domains coexist with chaotic seas in the real phase space.

In order to see the relation among the Laputa chain J^+ and $W^s(R)$ definitely, we take the initial manifold $\mathcal{A}_\alpha$ inside a rotation domain which is almost filled with KAM curves. To this end, it is convenient to choose $\mathcal{A}_\alpha$ as an invariant curve of the map linearized around the elliptic fixed point $E = (-\sqrt{a}, 0)$, which represents the harmonic vibration around the bottom of the cubic potential. As the parameter α labeling the initial manifold we take the 'action variable' of the invariant curve of the linearized map. Introducing the 'angle variable' $\varphi(\varphi \in \mathbb{R}, 0 \leqslant \varphi \leqslant 2\pi)$, the initial manifold is parametrized as

$$\mathcal{A}_\alpha = \{(q, p) | q = -\sqrt{a} - \sqrt{a\alpha/2r}\cos\varphi - \sqrt{a\alpha r/8}\sin\varphi - \sqrt{a},\ p = -\sqrt{a\alpha r/2}\sin\varphi\}, \tag{43}$$

where $r = \sqrt{4\sqrt{a}/(2-\sqrt{a})}$. $\mathcal{A}_\alpha$ is an ellipse and equation (43) well approximates a KAM circle by choosing a suitably small α. The chaotic regions exist either in the region bounded

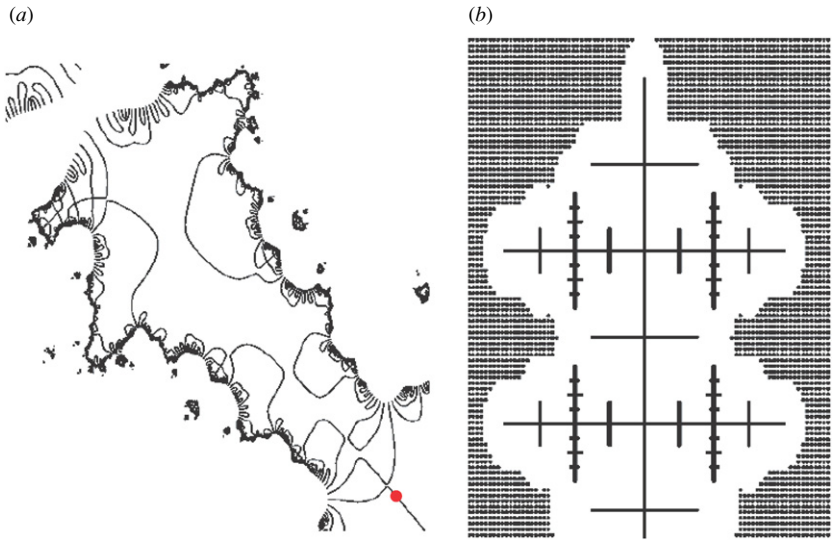

Figure 8. (*a*) Typical Laputa chains ($a = 0.64$) formed in the vicinity of the primary intersection between $\mathcal{A}_\alpha$ and the complexified $W^s(X)$ of a periodic saddle X in the chaotic sea in the real phase space. The red dot is the intersection. (*b*) The corresponding tree structure (schematic).

by KAM curves or in the outside region encircling the KAM curves. There exist no real trajectories linking $\mathcal{A}_\alpha$ and the surrounding chaotic regions. To describe the tunneling process, we complexify the angle variable as $\varphi = \xi + i\eta (\xi, \eta \in \mathbb{R})$. This just forms the initial value plane (ξ, η).

In the chaotic region encircling the KAM region, there are a series of periodic saddles rotating around the elliptic point E with increasing period. Let a real saddle be R, then the stable manifold of R can intersect with $\mathcal{A}_\alpha$ and Laputa chains emerge close to the intersection.

Figure 8 shows Laputa chains most dominantly contributing to the semiclassical propagator. Note that these emerge close to the primary intersection of $W^s(R) \cap \mathcal{A}_\alpha$. In this example, only the primary intersection for the period-5 (P5) saddle, which is the saddle with the shortest period in the real chaotic region, is plotted. (Note that there exist saddles of longer periods P6, P7, ... in the chaotic sea.) The homoclinic entanglement of stable and unstable manifolds for $P5$ generates a horseshoe, and they intersect with $\mathcal{A}_\alpha$ to form the Laputa chains in the same way as discussed in subsection 3.1. As shown in figure 8, bifurcations of the trunk chain into side chains, i.e., chains of higher order generations, also occur by the same mechanism as was described in section 3.2. Indeed, the side chains are formed close to the intersections with W^ss of longer periodic saddles P6, P7, ... according to the scheme (37), where P5 plays the role of R_1 and R_i with $i \geqslant 2$ are the longer period saddles such as P6, P7, etc. Many branches forming the chain of the first generation, of course, contribute to tunneling. Moreover, in the present case, even the branches forming the side chains of higher order generation contribute to the tunneling wavefunction due to the mechanism represented by the inequality (40). In fact, as shown in [17], numerical results confirm that the basic condition (39) is fulfilled if $\mathcal{X}_1$ is taken as P5 and $\mathcal{X}_N$ as P6, P7 etc, respectively. Thus the complex chaotic trajectories go first toward P5, are repelled by it, and finally land along $W^u(\mathrm{P6}) \cap \mathbb{R}^2$ and $W^u(\mathrm{P7}) \cap \mathbb{R}^2$, etc after an itinerary like (37).

We finally show that the trajectories from the first generation, which is close to the primary intersections of $W^s(\,\mathrm{P5})$ with $\mathcal{A}_\alpha$, control the tunneling probability. The primary intersection

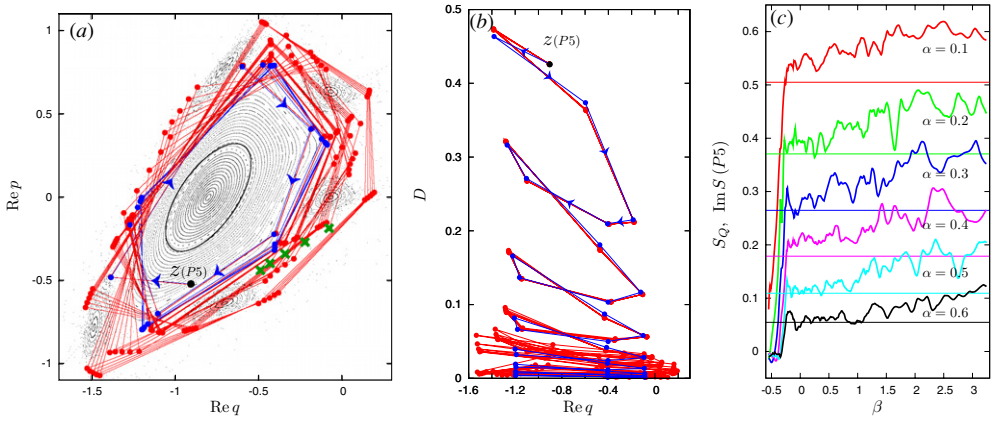

Figure 9. (*a*) and (*b*) Dominant tunneling trajectories (red) and the trajectory on W^s(P5) from $z(P5)$ (blue) spirally falling to the real plane: projection onto (*a*) (Re q, Re p) plane and onto (*b*) (Re q, D) plane. Poincaré plot (dots) and $\mathcal{A}_\alpha$ on $\mathbb{R}^2$ (black curve) are also plotted: $\alpha = 0.2$ (*c*): $S_n^{(Q)}(\beta)$ (thick curve) of the tunneling tail as a function of $\beta =$ Re q is compared with Im$S(P5)$ (thin line) for several initial states $\mathcal{A}_\alpha$ with increasing action α; $n = 40$, $a = 0.64$. This figure is taken from [5].

in $W^s(R) \cap \mathcal{A}_\alpha$ is here denoted by $z(R)$. The trajectories from many branches forming the first-generation chain all land along W^u(P5) $\cap \mathbb{R}^2$, resulting in complicated interference. This reflects the difference of Re $S_n^{(\ell)}$ in different branches. Since the first-order chain is localized in a close vicinity of z(P5), the tunneling probability from the chained branches can be approximated by

$$\left|K_n^{sc}(\alpha, \beta)\right| \sim \mathrm{e}^{-\mathrm{Im}S_{n=\infty}(z(\mathrm{P5}))/\hbar}, \tag{44}$$

where $S_{n=\infty}(z(R))$ is the action along the trajectory from $z(R)$, which approaches the saddle R along $W^s(R)$.

Figure 9 illustrates some of the most dominant tunneling trajectories together with the trajectory on W^s(P5) starting at z(P5). Figure 9(*a*) shows the projection of the trajectories onto $\mathbb{R}^2$, while figure 9(*b*) depicts the trajectories traced in the space of Re q and the distance $D = \sqrt{(\mathrm{Im}\ p)^2 + (\mathrm{Im}\ q)^2}$ from the real plane. In figure 9(*a*), the Poincaré plot and $\mathcal{A}_\alpha$ on $\mathbb{R}^2$ are also displayed for comparison with the tunneling trajectories. The dominant trajectories starting near z(P5) rotate following the trajectory on the complexified W^s(P5) and approach $\mathbb{R}^2$ exponentially. The former trajectories are then repelled by the latter trajectory and end (indicated by '**X**' colored by green in (a)) close to $\mathbb{R}^2$ on a well-defined curve, which is nothing more than a segment of $W^u(\mathrm{P5}) \cap \mathbb{R}^2$.

We remark that the trajectories leaving different branches land along different branches of $W^u(\mathrm{P5}) \cap \mathbb{R}^2$ forming the multiply folded structure. The correspondence between the entrance side (branches of the first-order chain) and the exit side (branches of $W^u(\mathrm{P5}) \cap \mathbb{R}^2$) is essentially the same as what we observed in the horseshoe limit, which is shown as figures 3(*a*) and (*b*).

Figure 9(*c*) shows the 'quantum action' $S_n^{(Q)}(\beta)$ for the fully quantum wavefunction, which is computed based on the numerical observation that the tunneling wavefunction depends on $\hbar$ as

$$|K_n(\alpha, \beta)| \propto \mathrm{e}^{-S_n^{(Q)}(\beta)/\hbar}. \tag{45}$$

Here we assume that the irregular oscillation peculiar to chaotic tunneling tail is removed by averaging over an appropriate scale of β. Note that, for a given initial manifold $\mathcal{A}_\alpha$, $\hbar$ is varied

discontinuously so as to satisfy the quantization condition $\hbar = [\text{area of } \mathcal{A}_\alpha \cap \mathbb{R}^2]/[2\pi(n+1/2)]$ (n: non-negative integer) because the quantum initial state should be on $\mathcal{A}_\alpha$. The quantum actions for initial quantum states on $\mathcal{A}_\alpha$ with various α are compared with Im $S_{n=\infty}(z(\text{P5}))$. The action Im $S_{n=\infty}(z(\text{P5}))$ explains the dominant part of the quantum action for all α. Significant deviation in the large $|\beta|$ regime is explained by the contribution from the complex chaotic trajectories launched at the higher generation branches, which contribute under condition (39). The role of higher generation branches will be reported elsewhere in detail [17].

Here, we have to remark that as long as the time step n is large but finite, $\mathcal{M}_n^{\alpha,\beta}$ contains additional components besides the components that converge to $\mathcal{A}_\alpha \cap J^+$. (See figures 1 and 2 in I and section 3.1 of I.) Within a finite n, such additional components are the majority of tunneling trajectories and the converging components are only a small fraction of all candidates. The majority of trajectories have no chance of approaching the real plane; rather they diverge to the deep imaginary domain. Thus Im S_n s along such trajectories are so large that they are negligible as semiclassical contributors.

In the above example the P5-saddle happens to give markedly smaller Im $S_{n=\infty}(z(R))$ compared with other saddles such as P6, P7, ..., but we should remark that sometimes multiple saddles can have almost the same value of Im$S_{n=\infty}(z(R))$. This provides another situation: several different Laputa chains with almost equal weights appear in the semiclassical propagator.

4. Fundamental hypothesis

In this section, we give an explanation of the results of sections 2 and 3, focusing on the fundamental role of complex-domain chaos implied by the results of Bedford and Smillie in the chaotic tunneling process.

4.1. Complex-domain chaos as basic transport mechanism

First of all, we consider the transport process through the complex phase space with several speculations that have not been mathematically proved but are numerically plausible.

A result of Bedford and Smillie is that the measure μ is mixing and in particular ergodic [8]. It is known that its support $J^* = \text{supp}\,\mu$ coincides with the Julia set J if g is hyperbolic. On the other hand, the best known property in the non-hyperbolic case is that

$$J^* \subset J. \tag{46}$$

Now, we shall take somewhat bold view for the purpose of physical explanations. We make the hypothesis that the following holds even in the non-hyperbolic case:

$$J = J^*. \tag{47}$$

Combining this hypothesis with the vacant interior conjecture, that is $K = J$, we reach the combined hypothesis:

$$J^* = J = K. \tag{48}$$

We explain the implications of this hypothesis in the context of our tunneling problem. As will be discussed in appendix B in detail, the KAM curves in the real phase space can be extended analytically into the complex domain and they are subsets of J under the vacant interior conjecture.

If $K = J^*$ holds, we conclude that any close neighborhood of complexified KAM curves are connected with each other via some orbits on K. This is because μ is mixing [8]: for

arbitrary neighborhoods $U(z_1)$ and $U(z_2)$ of any two points z_1 and z_2 in K respectively, there exists n such that $U(z_1) \cap g^n(U(z_2)) \neq \emptyset$.

Such transitivity of g in $\mathbb{C}^2$ makes a very sharp contrast to the dynamics confined in the real phase space, where any orbits bounded by KAM curves can never go out of the bounded region. If our working hypothesis is valid, *the mixing property of μ on J^* ensures the tunneling orbits travel among arbitrary pairs of sites on $K \cap \mathbb{R}^2$*, even if the two sites are in separate invariant sets, i.e., dynamically separated sets such as KAM circles and chaotic sets, in the real phase space.

The quantum tunneling allows the transition between any two neighborhoods. The above argument leads that such transitions, which usually understood as purely quantum effects, can be explained by the mixing of orbits in the complex space. In this sense, the classical transport in non-integrable systems and the tunneling transport in quantum non-integrable systems take place under the same mechanism.

In appendix B, we discuss how the torus in the real phase space can be extended into the complex phase space and show that the border of the complexified torus, the so-called *natural boundary*, is responsible for determining the initial position of dominant tunneling trajectories.

4.2. Tunneling paths: completely integrable versus non-integrable

The nature of complex chaos and its relation to complex paths controlling tunneling processes, partly proved rigorously and partly verified numerically, provide us with a unified view for the fundamental mechanism of chaotic tunneling, which is quite different from that of completely integrable systems. From the viewpoint of the quantum wave packet dynamics, the dynamical connection between the initial manifold $\mathcal{A}_\alpha$ and the final manifold $\mathcal{B}_\beta$, rather than individual orbitwise connection on J^* discussed in the previous subsection, is the central subject. Below we show that, if they are both algebraic sets, we have some strong statements on the formation of the tunneling paths between them based on the arguments in section 2.

From proposition 2.7 there exist subsequences $g^{-n_i}(\mathcal{B}_\beta) = \mathcal{M}_{n_i}^{*,\beta}$ for the forward evolution and $g^{m_j}(\mathcal{A}_\alpha) = \mathcal{L}_{m_j}^{\alpha,*}$ similarly for the backward evolution (more precisely $\hat{\mathcal{M}}_{n_i}^{*,\beta}$ and $\hat{\mathcal{L}}_{m_j}^{\alpha,*}$ taken in S^4, which is equivalent to $\mathbb{C}^2$), which have the limits with respect to the Hausdorff metric, and the limits $\lim_{n_i\to\infty} \mathcal{M}_{n_i}^{\beta}$ and $\lim_{m_j\to\infty} \mathcal{L}_{m_j}^{\alpha,*}$ contain J^+ and J^-, respectively. On the other hand, these two limits are respectively included by K^+ and K^- from equation (31) and lemma 2.11 (and 2.14). If the vacant interior conjecture $K^\pm = J^\pm$ is correct, these facts mean that $g^{-n_i}(\mathcal{B}_\beta)$ and $g^{m_j}(\mathcal{A}_\alpha)$ should converge to J^+ and J^-, respectively. Thus we can expect that for sufficiently large n_i and m_j, $g^{-n_i}(\mathcal{B}_\beta)$ and $g^{m_j}(\mathcal{A}_\alpha)$ intersect with each other in the close vicinity of $J^+ \cap J^- = J$. If $J = J^*$ holds, since μ is (weakly) hyperbolic and is also the maximal entropy measure, implying that the topological entropy on $J^*(= J)$ is positive, the number of intersections should be exponentially large with n_i and m_j, and so the same number of orbits which start at a given $\mathcal{A}_\alpha$ and end at a final $\mathcal{B}_\beta$ should exist. Let us consider the orbits connecting $\mathcal{A}_\alpha$ and $\mathcal{B}_\beta$ passing through the intersections $\mathcal{L}_{m_j}^{\alpha,*} \cap \mathcal{M}_{n_i}^{*,\beta}$. Since we can expect that $\mathcal{M}_{m_j+n_i}^{*,\beta}$ and $\mathcal{L}_{n_i+m_j}^{\alpha,*}$ are respectively well approximated by J^+ and J^-, the initial points $\left(\in \mathcal{M}_{m_j+n_i}^{*,\beta}\right)$ and the final points $\left(\in \mathcal{L}_{n_i+m_j}^{\alpha,*}\right)$ are very close to $J^+ \cap \mathcal{A}_\alpha$ and $J^- \cap \mathcal{B}_\beta$, respectively.

Thus we may expect that those trajectories leave $\mathcal{A}_\alpha$ guided by J^+, approach J (or J^*), and finally reach $\mathcal{B}_\beta$ along J^-. Such a process is symbolically expressed as

$$\mathcal{A}_\alpha \to J^+ \to J \to J^- \to \mathcal{B}_\beta. \tag{49}$$

Therefore the trajectories mimic chaotic trajectories wandering over J^* on their way from $\mathcal{A}_\alpha$ to $\mathcal{B}_\beta$. To be mathematically rigorous, such trajectories exist for certain sequences n_i ($\to \infty$) and m_j($\to \infty$), but extensive numerical observations suggest the following fundamental hypothesis:

For sufficiently large number of time steps there always exists an exponentially large number of trajectories connecting arbitrarily chosen $\mathcal{A}_\alpha$ and $\mathcal{B}_\beta$ and passing arbitrarily close to J.

These trajectories move along J^+, pass close to J and finally go along J^-. This is represented symbolically by (49). This scheme describes a generic feature of tunneling paths in non-integrable systems. The origin of this feature in the complex domain dynamics is the mixing property of complex-domain chaos on J^*, which is deduced from the theorem on the convergency of current. (Theorem 2.1. See also theorem 2.1 in [8].)

The transport mechanism discussed above is quite different from the instanton mechanism of tunneling in integrable systems, where the phase space is completely filled with complexified tori. (Namely, action-angle variables are complex valued.) The tunneling transport between $\mathcal{A}_\alpha$ and $\mathcal{B}_\beta$ occurs via complexified tori $\mathcal{T}$ intersecting both of them. In contrast to the scheme (49), the instanton mechanism is represented symbolically as

$$\mathcal{A}_\alpha \to \mathcal{T} \to \mathcal{B}_\beta. \tag{50}$$

In the nearly integrable regime, the tunneling is substantially dominated by the instanton mechanism [18], although the complex-chaotic transport mechanism also is expected to exist. The complex-chaotic mechanism becomes more manifest as the system goes far beyond the integrable regime.

Rigorous statements on the nature of chaos in complex phase space are known only for the family of polynomial mappings, and techniques used to prove theorem 2.1 may not be straightforwardly extended to more general cases such as transcendental mappings. The standard map is a paradigm system with generic bounded mixed phase space and in fact has been used as a model in our preceding paper [2, 4]. Even in such systems, there is evidence of the complex-chaos transport mechanism. Lazutkin and Simo have numerically investigated the complex phase space of standard and semi-standard maps and conjectured that the stable and unstable manifolds are densely distributed in the invariant set in complex phase space [19]. This is essentially the same as $\overline{W^s(p)} = J^+$ and $\overline{W^u(p)} = J^-$ in the Hénon map. We expect that the complex-chaos transport mechanism described above (49) holds widely for tunneling in non-integrable systems, and so we propose the fundamental hypothesis that it is a universal scenario for tunneling transport in chaotic systems.

5. Concluding remarks

In the preceding paper [1], we numerically investigated the characteristic set of initial values of the complex classical trajectories contributing to chaotic tunneling. This set was first discovered phenomenologically in [2] and called the Laputa chain. Key features of Laputa chains which were reported in part I were summarized in section 1 of this paper as the numerical observations (i)–(iii). We have confirmed that the features are common in all the non-integrable systems that we have examined so far, which strongly suggests that they are universal to tunneling trajectories in non-integrable systems. In particular, asymptotic natures of Laputa chains, summarized in numerical observations (ii) and (iii), were examined in part I, and these led us to an empirical definition of the Laputa chain and a new conjecture relating the Laputa chain with Julia sets, a key notion in the theory of complex dynamical systems. These conjectures were examined and developed in the present paper.

Fortunately, recent progress in the study of multi-dimensional complex dynamical systems has provided a set of fundamental results, especially with respect to the nature of invariant sets and their ergodic properties, which could be applied to our problem. Combining the empirical definition of Laputa chain and mathematically rigorous considerations, we arrived at a mathematical definition of the Laputa chain. The asymptotic convergence of the numerically observed 'shape' of the tunneling set was mathematically formulated in terms of the Hausdorff topology to obtain a limit set of convergent components. The Laputa chain $\mathcal{C}_{\text{Laputa}}$ was then defined as a subset of the limit set for which the associated trajectories have absolutely converging imaginary actions. With this definition, the relation between the Laputa chain, the forward filled Julia set K^+ and the forward Julia set J^+ was derived as the main theorem in section 1. The main theorem refers to three different situations of the Hénon map. In the most general case, the relation is claimed as $K^+ \supset \overline{\mathcal{C}_{\text{Laputa}}} \supset J^+$, which means that, on the entrance side, the most relevant complex trajectories are closely related to the forward Julia set J^+ which is well approximated by the stable manifold of any periodic saddle. Since the mathematical results use the potential theory, which at present is applicable only to the family of polynomial mappings, our rigorous assertions are limited to polynomial mappings (the quadratic map or the Hénon map in the present case). However, our numerical observations and similar analyses strongly suggest that the same is true for transcendental maps [19].

The claims in the main theorem hold in the asymptotic limit of infinitely many iteration steps. Moreover, depending on the nature of the Hénon map assumed in the main theorem, the relationship between Laputa chains and Julia sets is slightly different. Therefore, in section 3, we re-examined numerically in each of the three cases what the theorem physically implies for finite time steps. Under the strongest condition that the map shows a horseshoe in the real plane, the Laputa chain appears in an idealized form: every branch forming the Laputa chain has one-to-one correspondence to periodic saddles in the chaotic region in such a way that the tunneling trajectories from each branch approach exponentially to the corresponding saddle along its complexified stable manifold and eventually land close to its real unstable manifold. Thus the trajectories travel in the complex phase space schematically as $J^+ \to J \to J^-$, where J and J^- are the Julia set and the backward Julia set, respectively. Tunneling transport in complex phase space is most simply captured in this ideal model. This is the content of claim (iii) of the main theorem.

Once the horseshoe in the real plane is broken, the Julia set J is no longer confined to the real plane and it becomes a complex object. However, if the system is hyperbolic, there is still a close relationship between the dominant tunneling set and the Julia set J^+. This is claim (ii) of the main theorem. Guided by the theorem, we discovered the tunneling trajectories going around the *complex-domain chaos*. We discussed the conditions for observing complex chaos corresponding to quantum tunneling and concluded that the complex chaos may contribute to the formation of tunneling paths under some suitable conditions.

The most general case (i) of the main theorem covers most generic situations for which one usually discusses dynamical tunneling, but the claim is rather weak. However, we showed that it can be strengthened with the help of a numerically confirmed conjecture for $K^{\pm}$, called the vacant interior conjecture. The strengthened claim equation (42) then becomes the same as in case (ii) of the main theorem, and so the dominantly contributing tunneling set is closely approximated by J^+ in the same sense as in the hyperbolic case. Indeed, the numerical examination for the case with mixed phase space revealed that the stable manifold of periodic saddles in real chaotic sets plays a crucial role in the tunneling process, and that complex chaotic trajectories contribute as dominant tunneling paths.

The most non-trivial point in the assertions of Bedford and Smillie, which is far beyond the reach of numerical verifications, would be that the convergent theorem (theorem 2.1), and the

statements deduced from it, holds even if KAM curves and chaotic regions coexist in the real phase space. Even if the real phase space is decomposed into separate ergodic components, orbits are ergodic on the measure theoretic Julia set J^*. If we may further assume $J = J^*$ and the vacant interior conjecture, we can conclude that any neighborhood of a KAM curve is connected with any other neighborhoods via complex orbits on J. Therefore, as summarized in section 4, ergodicity or transitivity of chaos in the complex domain ensures tunneling transport in non-integrable systems: given any initial and final manifolds $\mathcal{A}_\alpha$ and $\mathcal{B}_\beta$, then there always exist an exponentially large number of tunneling paths, which is represented symbolically by the scheme $\mathcal{A}_\alpha \to J^+ \to J \to J^- \to \mathcal{B}_\beta$ (49). In this sense, the mechanism for the formation of tunneling paths in non-integrable systems is essentially a generalization of the mechanism found in the ideal horseshoe limit. This tunneling mechanism for non-integrable systems is in sharp contrast to the tunneling mechanism due to instantons in integrable systems $\mathcal{A}_\alpha \to \mathcal{T} \to \mathcal{B}_\beta$ (50). We stress that how the instanton mechanism is replaced by the chaotic tunneling mechanism with increase of the nonlinear parameter (a, in the case of the quadratic map) still remains an open question.

In addition to the above general framework, we also numerically explored the role of natural boundaries of complexified KAM curves and the relation to Laputa chains. We verified that the Laputa chains are located in the neighborhood of the natural boundary if the system is sufficiently non-integrable. The relation found here is far from rigorous, but the result suggests a particular relevance of the natural boundary.

Recently, it has been reported that a tunneling mechanism due to the complexified stable–unstable manifolds of real saddles works in a quite different situation, that is, multi-dimensional barrier tunneling in a continuous flow system [20, 21]. Movable singularities of the trajectories, which do not exist in discretized map systems, become crucial in the organization of tunneling paths in continuous time systems, but the resulting tunneling mechanism is essentially the same as the present one. Thanks to the simplicity of the situation, with no chaos in the real phase plane, a detailed analytical study could be performed and it has been shown that the mechanism results in a characteristic shape of the tunneling spectrum, which means that the dominantly contributing complex-classical trajectories land along the real unstable manifold according to the same scenario as the present one [21]. This allows us to be more confident that the tunneling mechanism due to complexified stable–unstable manifolds is universal in multi-dimensional tunneling processes.

The explanation of the transport mechanism in terms of the complexified stable and unstable manifolds provides a concrete recipe to give the tunneling amplitude for chaotic tunneling: the imaginary action evaluated along the stable manifold gives a representative imaginary action of a Laputa chain, and therefore our task is reduced to finding the stable manifold with minimal imaginary action. We stress that it is not still clear whether or not the stable manifold of only a single representative saddle dominantly contributes, like the example presented in section 3. The condition for a single stable manifold to win the competition is not clear. However, although there still remain such problems which need to be further elucidated, it does seem certain that the basic scheme of (49) is universal for quantum tunneling in chaotic systems.

We have shown how the semiclassical mechanism of quantum tunneling in non-integrable systems can be explained in terms of dynamics in the complex space. One may expect that quantum tunneling allows transitions to anywhere. However, actually, in integrable systems there is no tunneling between different tori. On the other hand, in non-integrable systems, tunneling to anywhere is supported by ergodicity of the orbits in the complex space. In this sense, the mechanism of quantum tunneling in non-integrable systems is similar for classical transport. Moreover, it is surprising that the connection between classical ergodicity and

quantum tunneling is provided by the Julia set, which previously had seemed to be only an abstract mathematical notion, with no relevance to the real physical world.

As mentioned above, there remain many technical challenges. However, this approach offers a big advance in our understanding of quantum tunneling in non-integrable systems to which there have not been systematic and efficient theoretical methods to approach.

Acknowledgments

The authors would like to thank K Takahashi and T Onishi for many discussions throughout this study. They are also grateful to E Bedford for helpful comments and suggestions on multi-dimensional complex dynamical system theory. They express thanks to S Tsuji for offering a very nice lodging where they discuss the present subject intensively. This work is supported by Grants-in-Aid for Scientific Research (C) No. 20340100 from the Ministry of Education, Culture, Sports, Science and Technology of Japan.

Appendix A. Vacant interior conjecture

Here we consider a sufficient condition for the vacant interior conjecture (41) by examining the 4D volume of $K^{\pm}$ in $\mathbb{C}^2$. Concerning the dynamics in $\mathbb{R}^2$, the set of non-escaping points contained in the rotation domain has a finite 2D volume according to the KAM theorem. Therefore, if we restrict $K^{\pm}$ to $\mathbb{R}^2$, they have interior points. On the other hand, in $\mathbb{C}^2$, the best known mathematical result for the volume of $K^{\pm}$ is

$$\mathrm{vol}(K^+) = \mathrm{vol}(K^-) < \infty \tag{A.1}$$

in the case of the area-preserving Hénon map [22].

Below we present numerical evidence implying the null 4D volume of $K^{\pm}$, which leads that $K^{\pm}$ have no interior points. To visualize the object in $\mathbb{C}^2$ phase space, we observe K^+ by taking its two-dimensional slices. In figure A1(a) we plot the initial points whose forward orbits are bounded. Thanks to the existence of filtering sets of the Hénon map (D and $V^{\pm}$ in equation (13)), we could precisely sort out the escaping trajectories by checking whether or not the trajectories are out of D up to a given finite step. The shape of 2D slice of K^+ changes as a position of the slice is shifted, but the following features are common. As observed in figure A1(a) the tree-shaped set of non-escaping points on each slice initially has seemingly non-vanishing thickness. With increase of time, however, the non-escaping set gradually becomes slim and shrinks to zero finally, though the rate of decrease of the non-escaping points is quite slow. To see the decay process of the non-escaping region closely, we plot the number of non-escaping points as a function of n. We prepare an ensemble of initial points around the stable elliptic fixed point $E = (-\sqrt{a}, 0)$, and measure the number of initial points whose trajectory does not escape to infinity. As shown in figure A1(b), the number of non-escaping initial points does not decrease initially, but it begins to decrease gradually beyond the initial stage and finally reaches a stationary stage in which an algebraic decreasing behavior is observed.

The origin of the slow escape is that trajectories tend to be trapped by the KAM circles which are continued analytically into the complex domain. Such an aspect discussed in detail in appendix B [4]. These numerical observations imply that K^+ has null 4D-volume. If this is the case, the 4D-volume of K^- is also null because, as is easily checked, the inverse of the area-preserving Hénon map is conjugate to the original area-preserving Hénon map, and so is the 4D-volume of $K = K^+ \cap K^-$. This implies that the filled Julia sets of the area-preserving

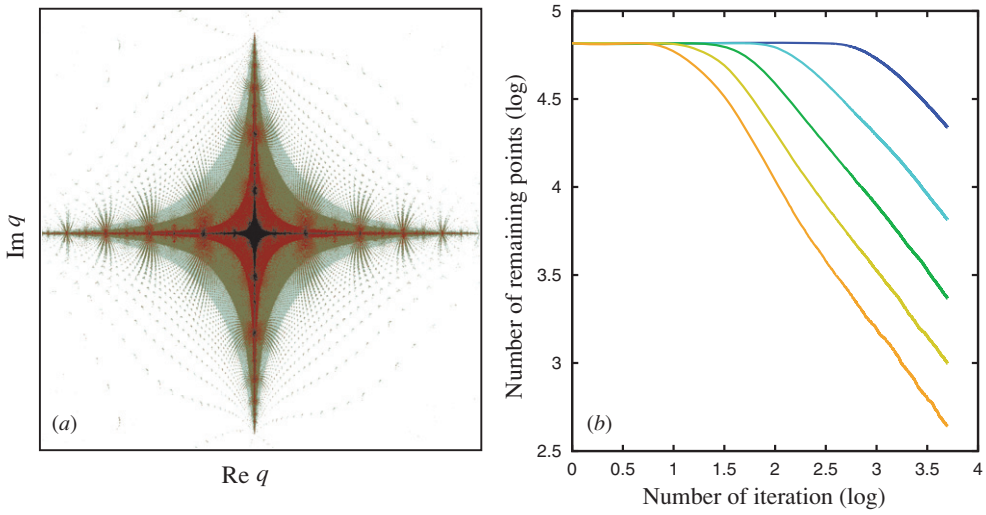

Figure A1. (*a*) The number of non-escaping orbits up to time step n. Initial points are placed on the boxes whose center is at a real fixed point of the map (3) with $a = 0.1$. The initial box size is given as 0.1, 0.2, 0.3, 0.4, 0.5 from the top to the bottom curves, respectively. (*b*) The slice of non-escaping points at $p - q = \sqrt{a}$ with $a = 0.9$. An elliptic fixed point is located at $(q, p) = (-\sqrt{a},0)$. In the order of color density, the maximum step is 500, 1000, 5000, 100 000, respectively. (These figures are taken from [5] with permission.)

Hénon map have null 4D-volume:

$$\mathrm{vol}(K^+) = \mathrm{vol}(K^-) = \mathrm{vol}(K) = 0,$$

which leads to the vacant interior conjecture (41).

The above numerical results are consistent with the fact that linearization around a fixed point is not possible in the area-preserving map. In the complex dynamical systems, it is known that rotation domains such as Siegel discs or Hermann rings, on which the dynamics is conjugate to a constant rotation around an equilibrium point, may appear under suitable conditions. The existence of the Siegel disc, for example, is related to the linearization problem, and the so-called non-resonance condition for the linearized matrix is required to give the Siegel disc. In the complex dynamics in $\mathbb{C}^2$, the linearized domain has a finite 4D-volume. If the linearization is possible around the fixed point, namely, if one can find an analytic conjugation map transforming the dynamics in a neighborhood of the elliptic fixed point into its linearized version, then $\mathrm{vol}(K^{\pm})$ turn out to be non-zero. However, it is obvious that this type of linearization is not possible in the area-preserving map, because we always have a pair of eigenvalues $e^{i\lambda}$ and $e^{-i\lambda}$ with $\lambda \in \mathbb{R}$, for the linearized map, which breaks the non-resonant condition necessary for the Siegel's construction of the conjugation map. All these suggest that the interior of the filled Julia set is vacant.

Appendix B. Natural boundaries and dominant tunneling paths

The mixing property on J^* guarantees the existence of complex paths between classically disconnected sets. However this does not tell us what sort of paths are actually selected in the tunneling transport. Indeed as described in section 3.3, if the initial manifold $\mathcal{A}_\alpha$ is taken such that its real component is fully inside the KAM domain, then the entrances of the dominant

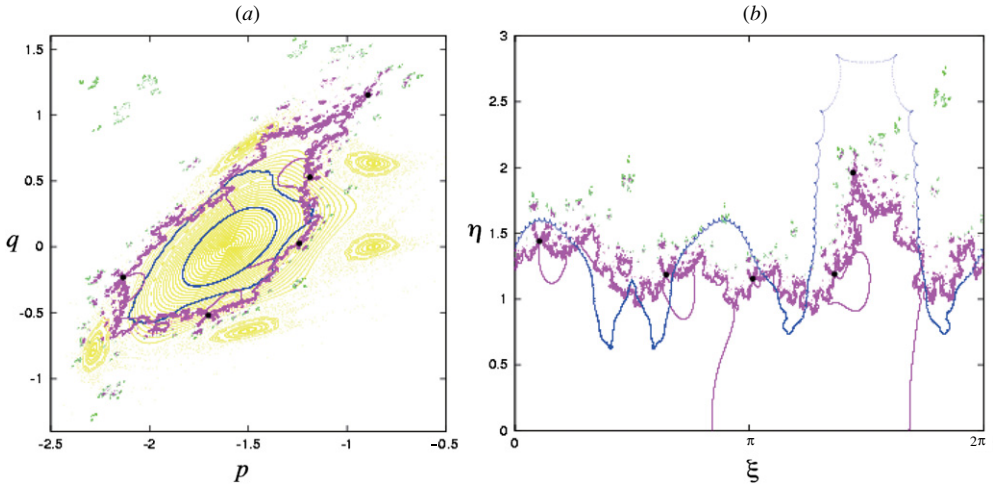

Figure B1. Comparison of the Laputa chains for an elliptic $\mathcal{A}_\alpha$ and the natural boundary of the KAM circle that best approximates $\mathcal{A}_\alpha$ on $\mathbb{R}^2$ ($a = 0.64$). (*a*) Projections onto the real phase plane: the KAM circle on $\mathbb{R}^2$ (blue), its natural boundary (blue), the set $\mathcal{M}_n^\alpha$ (purple) and Poincaré map on $\mathbb{R}^2$ (yellow). (*b*) Projections onto the angle variable space $\varphi = \xi + \mathrm{i}\eta$: the natural boundary (blue) and the set $\mathcal{M}_n^\alpha$(purple). In (*a*) and (*b*) the primary intersections of W^s(P5) with $\mathcal{A}_\alpha$ representing the positions of Laputa chains and the higher order intersections of W^s(P5) with $\mathcal{A}_\alpha$ are indicated by black circles and green dots, respectively.

tunneling paths, namely the Laputa chains, are located not close to the real phase space but deeply in imaginary domains as is shown in figures 8 and 9.

A basic question naturally arising here is what is responsible for determining the position of the entrances of the complex paths. The question exactly links to the argument about the role of *natural boundaries* of KAM curves, although some authors regard that their role not very active [24, 25]. It has been predicted that the extension of real KAM circles into the complex domain is interrupted and natural boundaries appear in general [23, 26]. Below we show that the entrances of the dominant tunneling paths from rotation domains are located in the neighborhood of the natural boundaries.

The KAM curve with rotation numbers ω can be expanded into the Fourier series of the angle variable φ

$$q = Q(\varphi) = \sum_{k=0}^{\infty} Q_k \, \mathrm{e}^{ik\varphi}, \qquad p = P(\varphi) = \sum_{k=0}^{\infty} P_k \mathrm{e}^{ik\varphi}, \tag{B.1}$$

which is absolutely convergent for $\varphi \in \mathbb{R}$, according to the Kolmogorov–Arnold–Moser theorem. KAM curves are not in general entire functions, and they have own finite radii of convergence. The Fourier coefficients $|Q_k|$ decay exponentially like $\mathrm{e}^{-\rho_c k}$, where $\rho_c > 0$ denotes the border of analyticity in the complex φ-plane. As numerically pointed out in [23], each Fourier series for a fixed ω has a natural boundary along which the singularities are distributed densely [26]. There is no way to continue analytically KAM circles beyond the border of analyticity[6]. Since a single forward iteration on the KAM invariant circle leads to a constant shift $\varphi \to \varphi + 2\pi\omega$, the mapping relation (3) requires the following functional equations to hold:

[6] In the case of the integrable system, ρ_c is determined by a simple pole or at most an isolated singularity with a fractional power and invariant circles can be extended analytically beyond ρ_c.

$$P(\varphi + 2\pi\omega) - P(\varphi) = -V'(Q(\varphi)), \tag{B.2}$$

$$Q(\varphi + 2\pi\omega) - Q(\varphi) = P(\varphi + 2\pi\omega), \tag{B.3}$$

which are solved by transforming them into a set of simultaneous algebraic equations for the Fourier coefficients [27].

To explore the relation between the natural boundary and the entrances of the tunneling paths, we take a certain KAM circle and an initial manifold $\mathcal{A}_\alpha$ that is entirely analytic but approximates the KAM circle reasonably well in the real plane. As given in equation (43), $\mathcal{A}_\alpha$ is chosen from an invariant circles of the linearized quadratic map. We compare the location of the natural boundary of a KAM circle with Laputa chains, the primary intersections $\mathcal{A}_\alpha \cap W^s(\mathrm{P5})$ and so on, which are associated with the entrances of the dominant tunneling paths on $\mathcal{A}_\alpha$.

First, in figure B1(a) we compare the projection of the natural boundary onto the real phase space with that of the primary intersection of $W^s(P5)$ with $\mathcal{A}_\alpha$. The projection of the set $\mathcal{M}_n^\alpha$ onto $\mathbb{R}^2$ is also displayed. The region occupied by the most contributing Laputa chains is localized very close to the intersection $W^s(P5) \cap \mathcal{A}_\alpha$. (Note that the region occupied by them is so small that they are hidden by the circle indicating the primary intersection.) One can see that the main Laputa chains are located around the natural boundary. Figure B1(b) gives the comparison using the complex action–angle coordinate $(\alpha, \varphi) \in \mathbb{C}^2$ defined by equation (43). (Note that, by definition, α is constant over $\mathcal{A}_\alpha$ and the set $\mathcal{M}_n^\alpha$ is specified only by the angle variable $\varphi = \xi + \mathrm{i}\eta$.) We confirm again that the primary intersection $W^s(P5) \cap \mathcal{A}_\alpha$ and the Laputa chains (they are also hidden by the circle indicating the intersections) are located in the neighborhood of the natural boundary.

The above observation suggests that the natural boundary is of particular importance for the tunneling transition in the KAM regions: the entrances of the dominant tunneling paths in the rotation domain are in the neighborhood of its natural boundary.

References

[1] Shudo A, Ishii Y and Ikeda K S 2009 *J. Phys. A: Math. Theor.* **45** 265101
[2] Shudo A and Ikeda K S 1995 *Phys. Rev. Lett.* **74** 682
Shudo A and Ikeda K S 1998 *Physica* D **115** 234
[3] Onishi T, Shudo A, Ikeda K S and Takahashi K 2001 *Phys. Rev.* E **64** 025201
[4] Shudo A, Ishii Y and Ikeda K S 2002 *J. Phys. A: Math. Gen.* **35** L225
[5] Shudo A, Ishii Y and Ikeda K S 2008 *Europhys. Lett.* **81** 50003
[6] Bedford E and Smillie J 1991 *Invent. Math.* **103** 69
[7] Bedford E and Smillie J 1991 *J. Am. Math. Soc.* **4** 657
[8] Bedford E and Smillie J 1992 *Math. Ann.* **294** 395
[9] Bedford E, Lyubich E and Smillie J 1993 *Invent. Math.* **112** 77
[10] Katok A 1980 *Publ. Math. L'IHÉS* **51** 137
[11] Fornæss J E and Sibony N 1992 *Duke Math. J.* **65** 345
[12] Bedford E and Smillie J 1992 *Ann. Math.* **160** 1
[13] Sterling D, Dullin H R and Meiss J D 1999 *Physica* D **134** 153
[14] Shudo A and Ikeda K S submitted
[15] Davis M J, MacKay R S and Sannami A 1991 *Physica* D **52** 171
[16] Arai Z 2007 *Exp. Math.* **16** 181
[17] Shudo A and Ikeda K S submitted
[18] Smith G C and Creagh S C 2006 *J. Phys. A: Math. Gen.* **39** 8283
[19] Lazutkin V F and Simo C 1997 *Int. J. Bifurcation Chaos Appl. Sci. Eng.* **2** 253
[20] Takahashi K and Ikeda K S 2001 *Found. Phys.* **31** 177
Takahashi K, Yoshimoto A and Ikeda K S 2002 *Phys. Lett.* **297** 370
Takahashi K and Ikeda K S 2003 *J. Phys. A: Math. Gen.* **36** 7953

[21] Takahashi K and Ikeda K S 2005 *Europhys. Lett.* **71** 193
Takahashi K and Ikeda K S 2008 *J. Phys. A: Math. Theor.* **41** 095101
[22] Morosawa S, Nishimura Y, Taniguchi M and Ueda T 1999 *Holomorphic Dynamics* (Cambridge: Cambridge University Press)
[23] Greene J M and Percival I C 1982 *Physica* D **3** 540
Percival I C 1982 *Physica* D **6** 67
[24] Creagh S C 1998 *Tunneling in Complex Systems* ed S Tomsovic (Singapore: World Scientific) p 35
[25] Brodier O, Schlagheck P and Ullmo D 2001 *Phys. Rev. Lett.* **87** 064101
Brodier O, Schlagheck P and Ullmo D 2002 *Ann. Phys., NY* **300** 88
[26] Berretti A and Chierchaia L 1990 *Nonlinearity* **3** 39
Berretti A and Marmi S 1992 *Phys. Rev. Lett.* **68** 1443
Berretti A, Celletti A, Chierchaia L and Falcolini C 1992 *J. Stat. Phys.* **66** 1613
[27] Shiromoto R, Shudo A and Ikeda K S in preparation